ELSEVIER

Contents lists available at ScienceDirect

# **Quaternary Science Reviews**

journal homepage: www.elsevier.com/locate/quascirev





# Changes in Indo-Pacific Warm Pool hydroclimate and vegetation during the last deglaciation

Meredith Parish<sup>a,\*</sup>, James Russell<sup>a</sup>, Bronwen Konecky<sup>b</sup>, Xiaojing Du<sup>c</sup>, Chengfei He<sup>d</sup>, Satria Bijaksana<sup>e</sup>, Hendrik Vogel<sup>f</sup>

- a Department of Earth, Environmental, & Planetary Sciences, Brown University, 324 Brook Street, Providence, RI, 02912, USA
- b Department of Earth, Environmental, and Planetary Sciences, Washington University in St. Louis, 1 Brookings Drive, St. Louis, MO, 63130 USA
- <sup>c</sup> Atmospheric, Oceanic & Earth Sciences Department, George Mason University, 4400 University Dr. Fairfax, VA, 22030, USA
- d Rosenstiel School of Marine, Atmospheric, and Earth Science, University of Miami, 4600 Rickenbacker Cswy, Key Biscayne, FL, 33149, USA
- <sup>e</sup> Global Geophysics Group, Faculty of Mining and Petroleum Engineering, Institut Teknologi Bandung, 4J66+CQ6, Lebak Siliwangi, Coblong, Bandung City, West Java, 40132. Indonesia
- f Institute of Geological Sciences & Oeschger Centre for Climate Change Research, University of Bern, Baltzerstrasse 1+3, 3012 Bern, Switzerland

### ARTICLE INFO

Handling Editor: Dr A. Voelker

Keywords: Leaf wax Indo-Pacific Warm pool Deglaciation Hydroclimate Precipitation

### ABSTRACT

Drying across much of the Indo-Pacific Warm Pool (IPWP) during the Last Glacial Maximum (LGM) has been widely recognized from interpretations of sedimentological, geochemical, and paleoecological records. Reconstructions of precipitation isotopic compositions have emerged as a powerful tool to reconstruct rainfall amount in many tropical regions, yet it has proven difficult to reconcile precipitation isotope records from the IPWP with records of widespread drying. To evaluate the signals preserved in precipitation isotope records, we produced new hydrogen and carbon isotope records from Lake Towuti and Lake Matano in Sulawesi, Indonesia using long-chain n-alkanes. We then compared these new records to existing n-alkanoic acid records from the same lakes and compiled available marine runoff, salinity, leaf wax hydrogen isotope (6<sup>2</sup>H<sub>wax</sub>), and leaf wax carbon isotope ( $\delta^{13}C_{wax}$ ) records in the IPWP. During the last deglaciation, marine runoff and salinity proxies reveal that precipitation amount began to increase dramatically between ~12.3 ka at the end of the Younger Dryas. A principal component analysis of precipitation isotope records indicates a shift from more <sup>2</sup>H-enriched to  $^2$ H-depleted waxes at  $\sim$ 12.3 ka as sea level rise inundates most of the Sunda and Sahul shelves, coincident with runoff and salinity proxies, suggesting precipitation isotopes respond strongly to rainfall amount in this region. Over 70% of IPWP  $\delta^{13}C_{wax}$  records show a transition from more to less  $^{13}C_{e}$ -enriched waxes beginning about 19.9 ka, prior to the reconstructed increases in precipitation. We suggest that vegetation shifted in response to the changing seasonality of precipitation. The dramatic changes in the IPWP during the last deglaciation highlight the capacity for the region to experience dynamic changes in precipitation, vegetation, and atmospheric circulation.

### 1. Introduction

The Indo-Pacific Warm Pool (IPWP) is the largest area of ocean with sea surface temperatures over 28 °C year-round and plays a vital role in shaping global climate. IPWP climate variations are highly consequential to the diverse ecosystems in the region and to the livelihoods of millions of people living on the Maritime Continent. Despite the region's importance, global climate model projections of future precipitation change over the Maritime Continent diverge (Iturbide et al., 2020).

Reconstructions of precipitation change over the past 30,000 year can provide valuable evidence to test the ability of global climate models to predict regional climate change and to determine the dominant forcings of rainfall variations in the IPWP under the changing boundary conditions from the Last Glacial Maximum (LGM), at 22 ka, to present.

Sedimentological and palynological records have provided qualitative but critical insights into past rainfall changes over the Maritime Continent, indicating widespread aridity at the LGM (Costa et al., 2015; Hamilton et al., 2019; Hope, 2001; Reeves et al., 2013; Russell et al.,

E-mail addresses: meredith\_parish@brown.edu (M. Parish), james\_russell@brown.edu (J. Russell), bkonecky@wustl.edu (B. Konecky), xdu5@gmu.edu (X. Du), cxh1079@miami.edu (C. He), satria@itb.ac.id (S. Bijaksana), hendrik.vogel@unibe.ch (H. Vogel).

<sup>\*</sup> Corresponding author.

2014; van der Kaars et al., 2000, 2001, 2010; Vogel et al., 2015). Isotopic records have provided powerful additional constraints on past climate. Carbon isotopes measured in leaf waxes ( $\delta^{13}C_{wax}$ ) generally show an expansion of C<sub>3</sub> plants during the last deglaciation, which has been attributed to extended and/or more arid dry seasons and/or reduced annual precipitation at the LGM relative to modern (Dubois et al., 2014; Ruan et al., 2019; Russell et al., 2014; Wicaksono et al., 2015, 2017; Windler et al., 2019; Wurster et al., 2019). Hydrogen isotope records from leaf waxes  $(\delta^2 H_{\text{wax}})$  and oxygen isotopes measured in speleothems ( $\delta^{18} O_{speleo})$  show more heterogeneous changes (Ayliffe et al., 2013; Griffiths et al., 2009; Konecky et al., 2016; Krause et al., 2019; Niedermeyer et al., 2014; Partin et al., 2007; Ruan et al., 2019; Tierney et al., 2012; Wicaksono et al., 2017; Windler et al., 2019; Wurtzel et al., 2018; Yuan et al., 2023). Precipitation isotopes can be directly simulated by isotope-enabled climate models and therefore provide a more direct test of paleoclimate model simulations, yet the existing isotope records from the IPWP show diverse patterns and present discrepancies with simulated precipitation isotopes during the LGM (Du et al., 2021). It is uncertain whether the differences among precipitation isotope records indicate complications with the proxies, or whether they arise from actual regional heterogeneity in precipitation isotopes across the IPWP. For instance, n-alkanoic acids have been used to reconstruct precipitation isotope at several sites in the region but could derive from aquatic as well as terrestrial sources (van Bree et al., 2018). However, paleoclimate model simulations suggest precipitation isotopes may vary substantially within the Maritime Continent and may record processes other than precipitation amount, due in part to exposure of the Sunda and Sahul shelves during times with lower sea level than the present day (Du et al., 2021). Unraveling the signals embedded in precipitation isotope records in this region thus requires careful interrogation of the proxies themselves, as well as local and regional changes in atmospheric circulation during the LGM and the ensuing glacial termination.

This study assesses differences between leaf-wax isotope records based on n-alkanoic acids and n-alkanes preserved in sediments from Lakes Towuti and Matano, Indonesia, and evaluates the spatiotemporal patterns in precipitation isotope records, marine runoff and sea surface salinity records, and  $\delta^{13}C_{\text{wax}}$  records across the Maritime Continent. We use runoff and salinity records to estimate the timing and patterns of precipitation change, and compare these to water isotope records to investigate the atmospheric circulation and water cycle changes recorded by these data. Additionally,  $\delta^{13}C_{\text{wax}}$  records enable us to investigate

changes in vegetation. The regional compilations of runoff, salinity,  $\delta^{18}O_{speleo}, \delta^2H_{wax}$  and  $\delta^{13}C_{wax}$  allow us to constrain the dominant drivers of hydroclimate and vegetation change in this region.

### 2. Regional Setting

Lake Towuti is a 560 km<sup>2</sup> lake located near the equator (2.75°S, 121.5°E) in central Sulawesi, Indonesia, a 174,600 km<sup>2</sup> island in the center of the IPWP (Fig. 1). Lake Towuti is at 318 m elevation, receives ~2700 mm of precipitation per year, and has a ~1644 km<sup>2</sup> watershed (Konecky et al., 2016; Russell et al., 2020). The majority of precipitation falls from February to May during the Australian-Indonesian summer monsoon season, with over 200 mm of precipitation per month sourced from the northwest (Konecky et al., 2016). Rainfall during the dry season (August to October), brought by winds from the southeast associated with the Asian summer monsoon, still averages over 50 mm of precipitation per month (Konecky et al., 2016). Lake Matano (2.5°S 121.3°E) is also located in Sulawesi, 10 km north of Lake Towuti. It is the deepest lake in Indonesia with a maximum depth of 590 m (Wicaksono et al., 2015). The catchment area has a mean altitude of 650 m and a lake-surface area of 276 km<sup>2</sup> (Wicaksono et al., 2015). HYSPLIT4 back-trajectory analysis indicates that air masses originate from the southeast during the June through October dry season and from the northwest in the November through May wet season, in addition to precipitation events sourced over local oceans (Konecky et al., 2016). Regionally, precipitation maxima migrate from northern Australia in December through January to southeast Asia in March through November (Figure A1). Precipitation minima migrate from southeast Asia in Boreal Winter to northern Australia in Austral Fall and Winter (Figure A1).

### 3. Methods

### 3.1. Modern precipitation isotopes

Konecky et al. (2016) presented monthly rain gauge and precipitation isotope measurements from 2013 to 2015. Here we present additional monthly modern isotope and rain gauge data, extending the study period from the beginning of the study in January 2013 into August of 2016. The rain gauge measurements and water samples were collected approximately ~8 km west of Lake Towuti in the village of Wawondula. Precipitation was collected as described by Konecky et al. (2016) and the

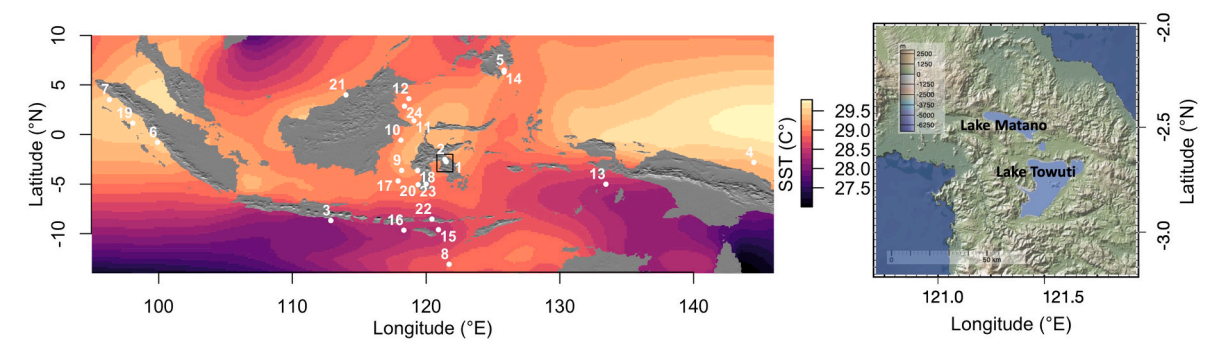


Fig. 1. Lake Towuti and Lake Matano are located on the island of Sulawesi near the middle of the Indo-Pacific Warm Pool. The map on the left shows nearby hydroclimate records that span the last deglaciation, numbered as follows: 1. Lake Towuti (this study; Konecky et al., 2016; Russell et al., 2014), 2. Lake Matano (this study; Wicaksono et al., 2015), 3. GeoB10053-7 (Mohtadi et al., 2011; Ruan et al., 2019), 4. GeoB17419-1 (Hollstein et al., 2018), 5. MD06-3075 (Fraser et al., 2014), 6. SO189-2\_039 KL (Mohtadi et al., 2014), 7. SO189-2\_119 KL (Mohtadi et al., 2014), 8. MD01-2378 (Sarnthein et al., 2011; Xu et al., 2008), 9. GIK18526-3 (Schröder et al., 2018), 10. GIK18519-2 (Schröder et al., 2018), 11. GIK18522-3 (Schröder et al., 2018), 12. MD98-2178 (Fan et al., 2018), 13. MD98-2176 (Stott et al., 2007), 14. MD98-2181 (Stott et al., 2002), 15. GeoB10069-3 (Dubois et al., 2014; Gibbons et al., 2014), 16. MD98-2165 (Levi et al., 2007), 17. MD98-2162 (Visser et al., 2003), 18. SO18515 (Wicaksono et al., 2017), 19. SO189-144 KL (Niedermeyer et al., 2014), 20. Gempa Bumi Cave (Krause et al., 2019), 21. Snail Shell and Bukit Assam caves (Partin et al., 2007), 22. Liang Luar Cave (Ayliffe et al., 2013), 23. SW Sulawesi caves (Yuan et al., 2023), and 24. 91GGC (Dubois et al., 2014). Mean annual sea surface temperatures (SST) from 1991 to 2021 from reanalysis data (Kalnay et al., 1996). SST and the digital elevation models are plotted using the "raster" package in R (Hijmans et al., 2022).

amount was measured every day with a Stratus RG202 Professional rain gauge. The water samples were sealed, refrigerated, and analyzed on a Picarro L1102-I Isotopic Water Liquid Analyzer at Brown University. We averaged the monthly rainfall over the entire study period and calculated the average isotopic composition of the rainwater by weighting the isotopic composition by the precipitation amount.

### 3.2. LGM, Early Holocene, and Pre-Industrial climate simulations

iTRACE is performed with the isotope-enabled Community Earth System Model version 1.3 (iCESM) (Brady et al., 2019), which is composed of the Community Atmosphere Model version 1.3 (CAM5.3), the Community Land Model version 4 (CLM4), Parallel Ocean Program version 2 (POP2), and Los Alamos Sea Ice Model, version 4 (CICE4). Here we used simulated precipitation amount and isotopic precipitation at the LGM (20.0–19.9 ka), the Early Holocene (11.1–11.0 ka), and Pre-Industrial (PI; 1850 CE) from the isotope-enabled Transient Climate Evolution (iTRACE) experiment, as described in Du et al. (2021) and He et al. (2021), to compare with our proxy record and instrumental observations from Lake Towuti. The Lake Towuti and Matano region is defined as extending from 1°S to 4°S and 120°E–123°E, which includes two grids cells that we averaged.

### 3.3. Sample preparation and analysis

The samples from Lake Towuti were taken from a piston core (IDLE-TOW10-9B) recovered from the center of Towuti's northern basin (Russell et al., 2014, 2020). There are 23 radiocarbon dates in the top 43 kyr of sediment (Russell et al., 2014), which we calibrated to Intcal20 and used to develop an age-depth model with Bacon in R (Blaauw and Christen, 2011) as described in Parish et al. (2023). Samples from Lake Matano were collected from IDLE-MAT10-5A. There are 10 radiocarbon dates in the top 46-kyr of sediment (Wicaksono et al., 2015), which we calibrated to Intcal20 and used to develop an age-depth model with Bacon in R (Blaauw and Christen, 2011).

Previous work (Russell et al., 2014; Wicaksono et al., 2015) extracted lipids from these sediments using a DIONEX Accelerated Solvent Extractor using dichloromethane:methanol (9:1). The lipid extract was divided into neutral and acid fractions using dichloromethane:isopropanol (2:1) and ethyl ether:acetic acid (96:4) over an aminopropyl silica gel column. Whereas prior work (Russell et al., 2014; Wicaksono et al., 2015) analyzed the isotopic composition of n-alkanoic acids, we focused on analysis of *n*-alkanes. To do so, we used silica gel columns to separate lipids within the neutral fraction, using hexane to isolate n-alkanes. We used silver thiolate columns to remove unsaturated compounds (Garelick et al., 2021; Ruan et al., 2019). We quantified the abundance of  $C_{29}$ ,  $C_{31}$ ,  $C_{33}$  n-alkanes using a gas chromatography flame ionization detector (GC-FID), and measured  $\delta^2H$  and  $\delta^{13}C$  of  $C_{29}$ ,  $C_{31}$ , and C<sub>33</sub> n-alkanes using a gas chromatography isotope ratio mass spectrometer (GC-IRMS).  $\delta^2$ H was measured in triplicate and  $\delta^{13}$ C was measured in duplicate on an Agilent 6890 GC with an HP1-MS column (30 m  $\times$  0.25 mm  $\times$  0.25  $\mu m$  ), coupled to a Thermo Delta Plus XL IRMS with a reactor temperature of 1425 °C for hydrogen and 1000 °C for carbon. A mixture of n-alkane standards from Arndt Schimmelmann (Indiana University) was injected every six samples to test for instrument drift and was used to correct the measured values to Vienna Standard Mean Ocean Water (VSMOW). The H3 factor was ~2 and stable during the analyses, suggesting no or minimal fluctuation in IRMS performance. Measured isotopic values were accepted if the voltage was between 3 and 8 V. From Lake Towuti, we analyzed 55 samples, spanning the past 30,000 years for an average sampling resolution of 1 sample every 567 years, with a minimum sampling resolution of 121 years and maximum sample resolution of 2197 years. From Lake Matano, we measured 31 samples over the past 32 kyr, resulting in an average sampling resolution of one sample every 986 years. The minimum sampling resolution was 314 years and the maximum sampling resolution was 2172 years. We measured  $\delta^{13}C_{wax}$  in both Towuti and Matano at about half the resolution of the  $\delta^2H_{wax}$  data. From Lake Towuti we measured 31 samples and we measured 14 samples from Lake Matano

#### 3.4. Leaf wax isotope corrections and interpretations

The  $\delta^2$ H of long-chain *n*-alkanes preserved in lake sediment generally reflects the isotopic composition of precipitation (Sachse et al., 2012). Longer chain length n-alkanes such as  $C_{31}$  alkanes are more likely to be derived from terrestrial leaf waxes than shorter chain length n-alkanes or n-alkanoic acids (Sachse et al., 2012; van Bree et al., 2018). Terrestrial plants take up meteoric water, derived from precipitation, to synthesize these epicuticular waxes, with an apparent fractionation between water and wax related primarily to evapotranspiration and biosynthetic fractionation. Because different plants have different apparent fractionation, it is common to correct the measured  $\delta^2 H_{wax}$  for changes in apparent fractionation to estimate the  $\delta^2 H$  of the precipitation ( $\delta^2 H_{\text{pre-}}$ cin) (Konecky et al., 2016; Lupien et al., 2021). Changes in apparent fractionation are often estimated from  $\delta^{13}C_{wax}$  values, which primarily record the relative abundances of plants that use the C3 and C4 photosynthetic pathways. Although this approach is common in the literature, we examined the apparent fractionation of C31 alkanes in plants using the C<sub>3</sub> and C<sub>4</sub> photosynthetic pathways from Sachse et al. (2012) taken within 30° of the equator and found no significant difference between C<sub>3</sub> and C<sub>4</sub> plants (Konecky et al., 2016; Figure A2). It is possible that a larger modern  $C_{31}$  alkane  $\delta^2$ H dataset could document a larger apparent fraction in C<sub>3</sub> plants; however, the existing C<sub>31</sub> alkane data indicates C<sub>3</sub> plants have a smaller (but not significantly different) mean apparent fractionation than C<sub>4</sub> plants (Hutchings and Konecky, 2020, 2022). Because we are unable to determine the apparent fractionation from existing data, we therefore used the average apparent fractionation of both C<sub>3</sub> and C<sub>4</sub> plants, rather than using an endmember mixing model, to estimate  $\delta^2 H_{precip}$ . The average fractionation of all tropical  $C_3$  and  $C_4$ plants is -135% for  $C_{31}$  alkanes (Sachse et al., 2012). The Towuti  $C_{28}$ alkanoic acid  $\delta^2 H_{wax}$  record was corrected using a constant offset of -129%, which is the average apparent fraction of all tropical  $C_3$  and  $C_4$ plants for C<sub>27</sub> alkanes (Sachse et al., 2012)

To help visualize changes in  $\delta^2 H_{precip}$  attributable to rainfall amount and atmospheric circulation, we corrected the  $\delta^2 H_{precip}$  for changes in seawater  $\delta^2 H$  by interpolating the global benthic  $\delta^{18} O$  stack (Lisiecki and Raymo, 2005) to the resolution of our measurements. To do so, we scaled the  $\delta^{18} O$  stack values to account only for the change attributable to changing ice volume (Schrag et al., 1996), converted  $\delta^{18} O$  to hydrogen space using the global meteoric water line, and subtracted the effect of the change in the isotopic composition of global seawater from the measured  $\delta^2 H_{Drecip}$ .

# 3.5. Proxy record synthesis

We compiled all regional runoff,  $\delta^{18}O$  of sea water ( $\delta^{18}O_{SW}$ ),  $\delta^{18}O_{speleo},\,\delta^2H_{wax},\,$  and  $\delta^{13}C_{wax}$  records in the IPWP that span the last deglaciation. We only included records that had at least three age controls between 20 and 12 ka and that span 21 ka to 2 ka,  $\delta^{18}O_{sw}$  records were produced using identical methods as Gibbons et al. (2014). Briefly, sea surface temperatures (SST) were used to convert the  $\delta^{18}O_{calcite}$  records to  $\delta^{18}O_{sw}$  using the following equation, where a = 16.5  $\pm$  0.2 °C, b =  $-4.80\pm0.16$  °C, and T is the measured SST:

$$\delta^{18}O_{sw} = -\,T\big/b + a\big/b + \delta^{18}O_{calcite}$$

Then, a 0.27% adjustment was used to convert the records from VPDB to VSMOW, and isotopic changes in seawater driven by ice volume were removed.  $\delta^{18}O_{speleo}$  measurements were converted to  $\delta^2H$  values assuming  $\delta^{18}O_{speleo}$  directly record precipitation isotopes, with no impact of changes in cave temperature, and scaling the  $\delta^{18}O_{speleo}$ 

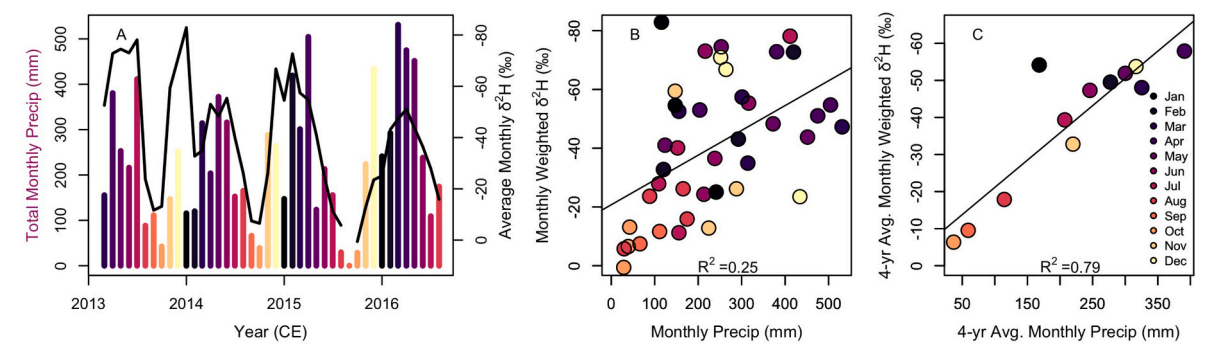


Fig. 2. A) Monthly rain gauge and precipitation isotope data from Lake Towuti from 2013 to 2016. B) Linear regression of the monthly precipitation amount and  $\delta^2$ H. C) Linear regression of the average monthly precipitation amount and weighted  $\delta^2$ H from 2013 to 2015 measurements from the rain gauge.

using the global meteoric water line. To detect the dominant modes of variability in the data, we performed both a principal component analysis (PCA) and stacking (averaging) of each set of proxy records after interpolating all records to a common timestep. The timestep was the mean resolution of all the records.

Using the  $\delta^{13}C_{wax}$  we calculated the percentage of  $C_3$  plants contributing to the sedimentary leaf wax pool using the mixing model described in Konecky et al. (2016). The median  $\delta^{13}C$  composition of  $C_3$  and  $C_4$  plants calculated from the n-alkanes of tropical plants were used as the endmembers in the mixing model. In the tropics,  $C_3$  plants have a median  $\delta^{13}C$  of  $C_{31}$  n-alkanes of  $-35.9 \pm 2.2\%$  (median  $\pm$  standard deviation, n=20) and  $C_4$  plants have  $\delta^{13}C$  of  $C_{31}$  n-alkanes of  $-22.1 \pm 2.6\%$  (median  $\pm$  standard deviation, n=12; Figure A2; Sachse et al., 2012).

### 3.6. Changepoint detection

We used the EnvCpt package in R to identify changepoints in the trend (slope) in all of the compiled hydroclimate records (Killick et al., 2021). The changepoints were determined by calculating stepwise linear functions that minimize the total residual error. We interpret the changepoint detected between 22 and 8 ka in each set of records as the timing of a deglacial changepoint, confirmed by visual inspection of the proxy data. We determined the uncertainty of the timing of each changepoint, using Bacon to recalibrate the published radiocarbon dates to IntCal20 and calculate the age uncertainty (Blaauw and Christen, 2011).

### 4. Results

### 4.1. Modern climatology and precipitation isotopes

From January 2013 to August 2016, the individual monthly isotopic composition of the collected precipitation is correlated, albeit weakly, with precipitation amount ( $R^2=0.25;\,p<0.01;\,Fig.~2B$ ). Precipitation amount and its isotopic composition are highly correlated when averaging the monthly values from the entire study ( $R^2=0.79;\,p<0.01;\,Fig.~2C$ ). The positive correlation between 2013 and 2015 rain gauge measurements from Lake Towuti and precipitation data from the region (Konecky et al., 2016) indicates that precipitation at Lake Towuti is representative of central Sulawesi precipitation, which itself is correlated to precipitation variations over a large region of central and southern Indonesia (Konecky et al., 2016).

# 4.2. Simulated LGM, Early Holocene, and PI climatology and precipitation isotopes

In the iTRACE simulation, the seasonal patterns of precipitation are somewhat similar to modern observations, though iTRACE simulates substantially less seasonality during the PI than we observe during the present-day. The model simulates wet conditions through much of the year, but with an ASO dry season, similar to the modern observations (Fig. 3C). The monthly precipitation modeled by the PI iTRACE simulation is moderately correlated with  $\delta^2 H_{\text{precip}}$  (R<sup>2</sup> = 0.31; p = 0.06; Fig. 3D). The monthly precipitation amount simulated with the PI iTRACE simulation is not strongly correlated with the modern 4-yr average (R<sup>2</sup> = 0.27; p = 0.09). The simulated  $\delta^2 H_{precip}$  is strongly correlated with the average from the modern 4-yr study ( $R^2 = 0.69$ ; p < 0.01). Although the seasonality of precipitation is not simulated well in the area around Lake Towuti, the model's performance is satisfactory across the larger Asian monsoon region (He et al., 2021). During the LGM, the model simulates substantially less precipitation than in the modern, with a particularly large reduction in precipitation during the ASO dry season relative to preindustrial (Fig. 3G). The isotopic composition of precipitation has a similar seasonality to the observations in the PI, Early Holocene, and LGM, and it is positively correlated with precipitation amount in the LGM simulation ( $R^2 = 0.76$ ; p < 0.01; Fig. 3H). The iTRACE-simulated Early Holocene precipitation shows precipitation maxima in June and December-January (Fig. 3E). Precipitation amount is only moderately correlated with the isotopic composition of rainwater during the Early Holocene ( $R^2 = 0.32$ ; p < 0.01; Fig. 3F). Precipitation during the dry season greatly increased during the Early Holocene, compared to at the LGM (Fig. 3). The transient iTRACE simulations shows that the percent of dry season (ASO) precipitation on Sulawesi increases from  $\sim$ 15% at the LGM to  $\sim$ 18% in the Early Holocene and  $\sim$ 35% in the PI (Fig. 3I).

### 4.3. Lake Towuti and Lake Matano leaf-wax isotope records

Variations in the relative abundance of different n-alkanes can provide information about the sources of these lipids. The carbon preference index (CPI) can be used to assess the state of preservation of the alkanes, wherein fresh vegetation can have a CPI of 6 or higher and a CPI of  $\sim 1$  indicates that the hydrocarbons in a sample are highly degraded and potentially from oil (Bray and Evans, 1965). The average carbon preference index (CPI) value of the Towuti samples was 3.3, with a maximum of 4.8 and minimum of 2.6. The average CPI value from Matano was 4.0, with a maximum value of 5.8 and a minimum value of 2.6. Overall this indicates the n-alkanes were well-preserved. The average chain length (ACL) calculated for C25 to C33 from Towuti was 29.5, with a maximum of 30.0 and a minimum of 28.5. The average ACL from Matano was 29.7, with a maximum of 30.5 and a minimum of 27, indicating the n-alkanes are most likely derived from terrestrial plants.

The Towuti  $C_{29}$ ,  $C_{31}$ ,  $C_{33}$   $\delta^2 H_{wax}$  records (not corrected for vegetation and ice volume) show  $^2 H$ -enrichment at the LGM relative to the  $^2 H$ -depletion in the Holocene (Fig. 4A). All of the homologues show a similar structure and amplitude of change.  $C_{31}$   $\delta^2 H_{wax}$  is positively correlated with  $C_{29}$   $\delta^2 H_{wax}$  ( $R^2 = 0.64$ ; p < 0.01) and  $C_{33}$   $\delta^2 H_{wax}$  ( $R^2 = 0.30$ ; p < 0.01). The greatest differences between homologues occurs between 30 and 26 ka, when  $C_{29}$   $\delta^2 H_{wax}$  is more  $^2 H$ -depleted than  $C_{31}$ 

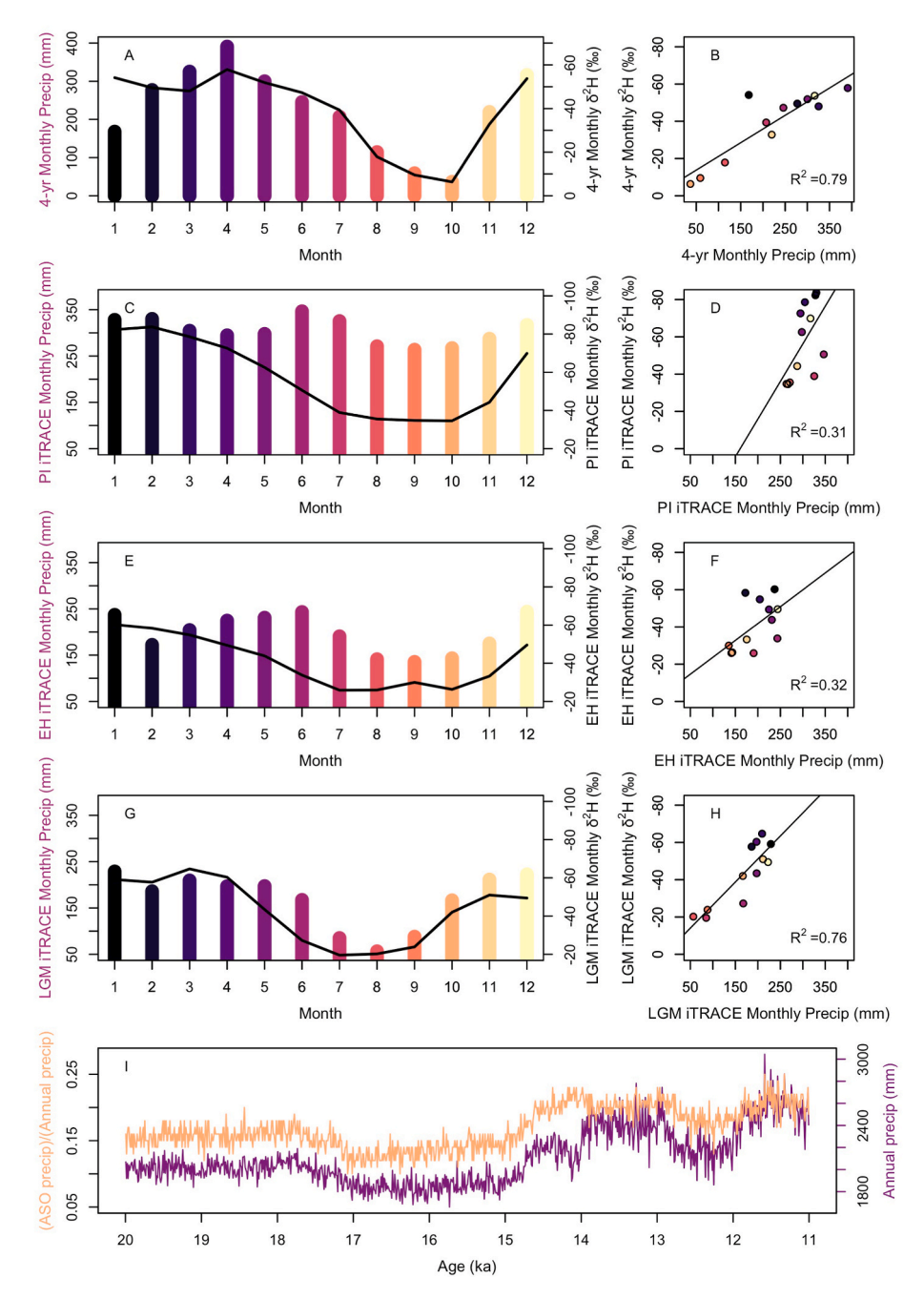


Fig. 3. A) Monthly average precipitation and isotopic composition from the 2013–2015 study period and B) the associated linear regression. C) Monthly iTRACE-simulated difference between precipitation amount and precipitation isotopic composition at the Pre-Industrial (PI, 1850 CE) and D) the linear correlation, E) Last Glacial Maximum (LGM, 20–19.9 ka) and F) the linear correlation, and G) the Early Holocene (EH, 11.1–11.0 ka) and H) the linear correlation. I) The transient evolution of the ASO fraction of annual precipitation and annual precipitation.

and  $C_{33}$   $\delta^2 H_{wax}$  (Fig. 4A). Like Towuti, the uncorrected  $C_{31}$   $\delta^2 H_{wax}$  record from Lake Matano shows  $^2 H$ -enrichment at the LGM and  $^2 H$ -depletion during the Holocene, but the shift is smaller than observed at Lake Towuti (Fig. 4C). The uncorrected Matano  $C_{29}$   $\delta^2 H_{wax}$  record shows the greatest magnitude of change from the LGM to the Holocene. The  $C_{33}$   $\delta^2 H_{wax}$  record has considerable  $^2 H$ -depletion at  $\sim$ 9.5 ka, which is not reflected in the other homologues. The shift to  $^2 H$ -depleted values in the Holocene in all of the homologues occurs about 12 ka, more than 5 kyr after the onset of deglacial warming on Sulawesi recorded from this same set of samples in Lake Towuti (Parish et al., 2023).

After correcting the  $\delta^2 H_{wax}$  values for ice volume and the isotopic fractionation by plants, the resulting  $\delta^2 H_{precip}$  indicates similar isotopic compositions during the LGM and Holocene with the most  $^2 H_{-}$ 

enrichment occurring at 12 ka (Fig. 5A). Using an end-member mixing model (Konecky et al., 2016), rather than our constant apparent fractionation, to estimate apparent fractionation and to correct the  $\delta^2 H_{\text{wax}}$  to  $^2 H_{\text{precip}}$  does not considerably impact the  $\delta^2 H_{\text{precip}}$  records (Figure A7). The Towuti n-alkane-based  $\delta^2 H_{\text{precip}}$  record and the n-alkanoic acid based  $\delta^2 H_{\text{precip}}$  record (Konecky et al., 2016) share common trends (Fig. 5A). Both records are slightly more  $^2 H$ -depleted during the LGM and during the Holocene and more  $^2 H$ -enriched between 17ka and 10 ka. The n-alkane and n-acid records are not strongly correlated when including all individual measurements (R $^2 = 0.08$ ; p > 0.05). However, calculating the correlation between the 2000-yr moving averages to smooth the data results in a stronger correlation (R $^2 = 0.36$ ; p = 0.02).

The similarity between the alkane  $\delta^2 H_{precip}$  record from nearby Lake

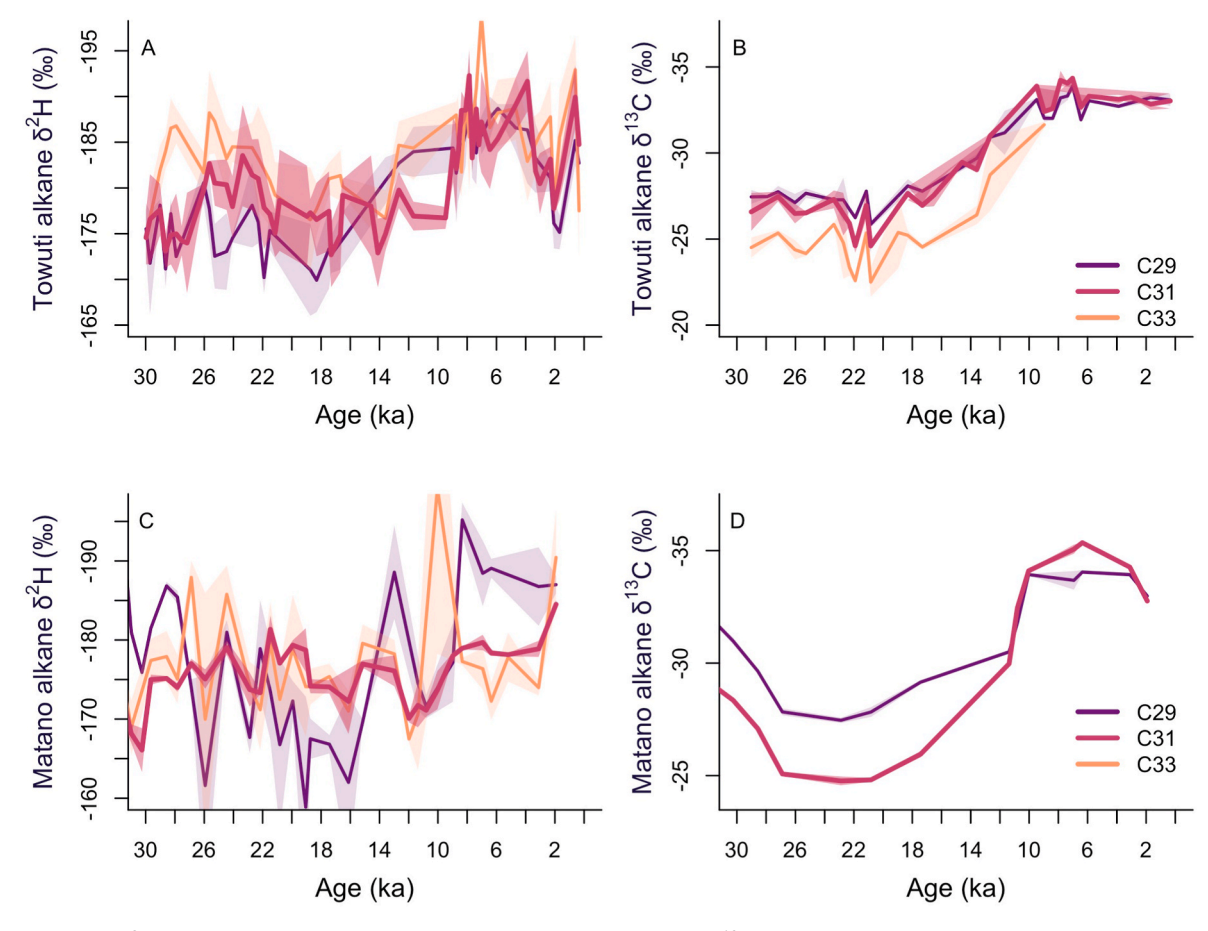


Fig. 4. A) Uncorrected  $\delta^2 H_{wax}$  of  $C_{29}$ ,  $C_{31}$ , and  $C_{33}$  alkanes measured from Lake Towuti. B)  $\delta^{13} C_{wax}$  of  $C_{29}$ ,  $C_{31}$ , and  $C_{33}$  alkanes measured from Lake Matano. D)  $\delta^{13} C_{wax}$  of  $C_{29}$  and  $C_{31}$  alkanes measured from Lake Matano.

Matano and the Lake Towuti  $\delta^2 H_{precip}$  record supports the interpretation that the records reflect the isotopic composition of the rainwater received by terrestrial plants over the past 30 kyr. The different absolute values between the alkane and acid records at Lake Towuti may be due to aquatic contributions to C28 n-acid (van Bree et al., 2018). In principle, if the *n*-alkanoic acids were produced by aquatic plants that reflect the isotopic composition of the lake water, we might expect the n-alkanoic acids to be more  $^2$ H-enriched than the terrestrial n-alkanes, particularly in samples from the LGM when the region experienced drying (Russell et al., 2014) and the lake level was ~30 m lower than present (Vogel et al., 2015). However, we do not observe <sup>2</sup>H-enrichment of acids relative to alkanes during the LGM compared to the Holocene. Temperate sites have reported n-alkanes that are 30% more depleted than n-acids (Chikaraishi and Naraoka, 2007; Hou et al., 2008). However, in samples from the Amazon and Andes there is not a significant difference between  $C_{30}$  acids and  $C_{29}$  alkanes (Feakins et al., 2016). The differences between the n-acid and n-alkane records may be due to differences in apparent fractionation for which we cannot account, particularly given the uncertainty in sources for C<sub>28</sub> n-acid to tropical lake sediments (van Bree et al., 2018).

The C<sub>29</sub>, C<sub>31</sub>, C<sub>33</sub>  $\delta^{13}$ C records from Towuti show shifts from  $^{13}$ C-enrichment at the LGM to  $^{13}$ C-depletion during the Holocene. C<sub>29</sub>  $\delta^{13}$ C shows a ~6% shift from ~27 to ~33%, C<sub>31</sub>  $\delta^{13}$ C shows a ~7% change from ~26 to ~33%, and C<sub>33</sub>  $\delta^{13}$ C shows a ~8% change from ~24 to ~32% (Fig. 4B).  $\delta^{13}$ C n-alkane and n-acid records from Lake Towuti are similar throughout the past 30 kyr, though the n-acid record is more depleted during the Holocene than the alkane record (Fig. 5B). At Lake Matano, the C<sub>31</sub>  $\delta^{13}$ C record shows a ~9% change, from ~24% at the LGM to ~35% in the Holocene, and the C<sub>29</sub>  $\delta^{13}$ C record shows a slightly smaller amplitude change (Fig. 4D). The structure of LGM-to-Holocene

change in the Matano  $C_{29}$  and  $C_{31}$   $\delta^{13}C$  records is similar to the  $C_{26}$  and  $C_{28}$   $\delta^{13}C$  records from Matano (Fig. 5c; Wicaksono et al., 2015). However, the  $C_{26}$  and  $C_{28}$  n-acids from Matano are more  $^{13}C$ -depleted for the last 20 kyr than at Towuti and show a smaller amplitude of change from the LGM to the Holocene. It is unclear why the n-acid amplitude of change in  $\delta^{13}C$  is greater than n-alkanes at Towuti and less than n-alkanes at Matano (Fig. 5B and C). The acid record may have non-terrestrial contributions (van Bree et al., 2018). Alternatively, different plants produce different relative abundances of alkanes and acids (Contreras et al., 2023).

### 5. Discussion

### 5.1. Surface runoff and precipitation during the deglaciation

Our syntheses of proxy reconstructions of rainfall, precipitation isotopes, and geochemical records of vegetation provide new insight into IPWP paleoclimate dynamics and the sensitivity of vegetation to rainfall. We rely on indicators of precipitation change other than precipitation isotopes and vegetation to help elucidate rainfall history and its influences on IPWP precipitation isotopes and ecosystems. Specifically, we synthesized four surface runoff records and 12 salinity records in the IPWP as recorders of precipitation amount. There are four marine and lacustrine geochemical runoff records in the IPWP with at least three age controls between 20 and 12 ka and that span 21 to 2 ka (Table 1; Costa et al., 2015; Fraser et al., 2014; Hollstein et al., 2018; Mohtadi et al., 2011). The two marine records of ln(Ti/Ca) (Hollstein et al., 2018; Mohtadi et al., 2011), one marine record of log(Fe/Ca) (Fraser et al., 2014), and one lacustrine Ti concentration record (Costa et al., 2015) included in our synthesis, assume that rainfall is the

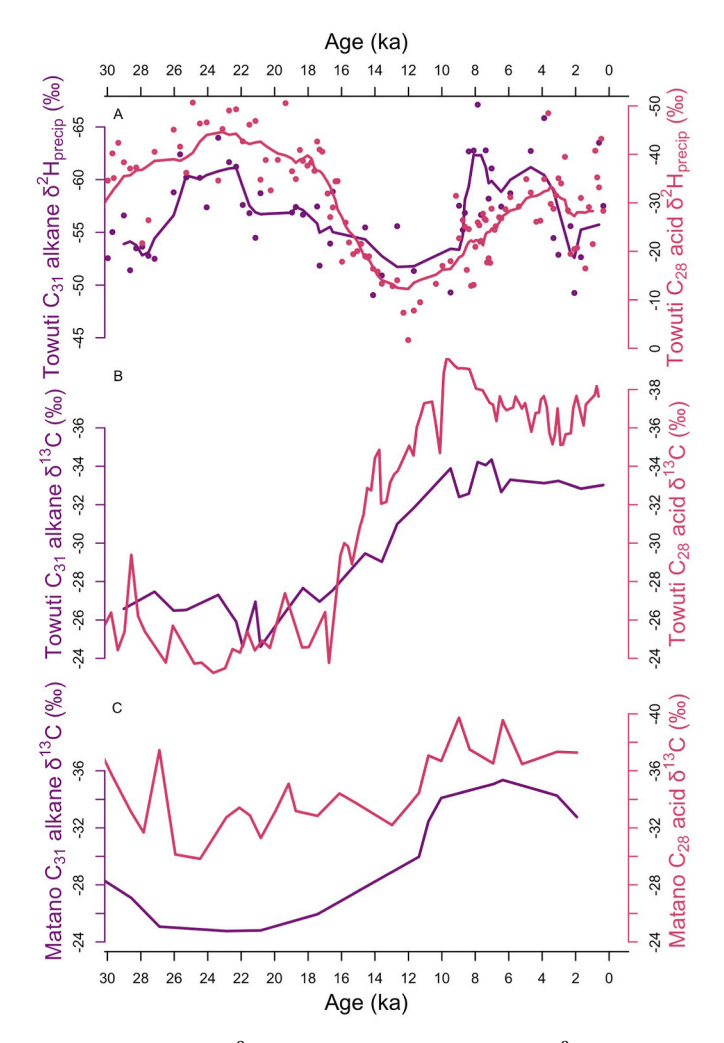


Fig. 5. A) Lake Towuti  $\delta^2 H_{precip}$  of  $C_{31}$  n-alkanes (purple) and  $\delta^2 H_{precip}$  of  $C_{28}$  n-acids (pink) corrected for changes in ice volume and vegetation. The solid line is a 2000-yr moving average. B) Lake Towuti  $\delta^{13}$ C of  $C_{31}$  n-alkanes (purple) and  $C_{28}$  n-alkanoic acids (pink). C) Lake Matano  $\delta^{13}$ C of  $C_{31}$  n-alkanes (purple) and  $C_{28}$  n-alkanoic acids (pink).

dominant control on erosion, which supplies Ti and Fe to sediments. Changepoint analysis of the four runoff records (Killick et al., 2021) shows that Ti began to increase at between 14.7 and 9.1 ka with an average of 12.4 ka (Table 1; Fig. 10).

There are  $12 \ \delta^{18}O_{sw}$  records in the IPWP with at least three age controls between 20 and 12 ka and span 21 to 2 ka (Table 1; Fan et al., 2018; Gibbons et al., 2014; Levi et al., 2007; Mohtadi et al., 2010; Rosenthal et al., 2003; Sarnthein et al., 2011; Schröder et al., 2018; Stott et al., 2002, 2007; Visser et al., 2003; Xu et al., 2008).  $\delta^{18}O_{sw}$  is a proxy for sea surface salinity and rainfall isotopic composition (Gibbons et al., 2014). Changepoint analysis indicates that shift to more isotopic depletion and likely decreased salinity begins at an average of 12.3 ka, with the earliest record shifting at 15.2 ka and the latest record shifting at 10.8 ka (Table 1; Fig. 10).

The first principal component (PC1) and the mean of the 16 z-scored runoff and  $\delta^{18}O_{sw}$  records indicate two pulses of decreased precipitation at  $\sim\!16$  and  $\sim\!12.5$  ka, followed by a shift to increased precipitation during the Holocene (Fig. 6C). Although the LGM is characterized by depleted isotopic compositions and decreased runoff relative to Heinrich Stadial 1 ( $\sim\!19\text{-}15$  ka) and the Younger Dryas ( $\sim\!12.9\text{-}11.7$  ka), there is an overall shift to more depleted  $\delta^{18}O_{sw}$  and increased runoff from the LGM to the Holocene that may be attributed to increased precipitation.

These observations are supported by increasing mean grain size during the last deglaciation in a marine record from southern Java, which Mohtadi et al. (2011) interpreted to reflect increased river runoff in the region from the LGM to the Holocene, with even drier periods than the LGM at Heinrich Stadial 1 and the Younger Dryas.

There are potential confounding influences on runoff and salinity proxies. Ln(Ti/Ca) can be affected by changes in sea level and production and preservation of calcium carbonate, the main source of Ca to sediment.  $\delta^{18}O_{sw}$  can reflect the isotopic composition of rainwater in addition to surface freshwater balance. For instance, Gibbons et al. (2014) suggest that the relatively salty (enriched) compositions observed during Heinrich Stadial 1 (~19-15 ka) and the Younger Dryas (~12.9-11.7 ka) were caused by a distinct isotopic composition of precipitation due to shifts in the position of the ITCZ, in addition to changes in precipitation amount. However, variations in the isotopic composition of precipitation are likely to be small relative to the isotopic difference between the ocean and rainfall, such that  $\delta^{18}O_{sw}$  should primarily trace rainfall amount. The amplitude of shifts toward enriched  $\delta^{18}O_{sw}$  during Heinrich Stadial 1 and the Younger Dryas are very large, and could mask the transition from the LGM to the Holocene. However, the  $\delta^{18}O_{sw}$  records still indicate that the LGM is saltier (more enriched) than the Holocene.

### 5.2. Precipitation isotope records

 $\delta^{18}O_{speleo}$  and  $\delta^{2}H_{wax}$  records show heterogeneous precipitation isotope changes within the IPWP (Ayliffe et al., 2013; Griffiths et al., 2009; Konecky et al., 2016; Krause et al., 2019; Niedermeyer et al., 2014; Partin et al., 2007; Ruan et al., 2019; Wicaksono et al., 2017; Wurtzel et al., 2018; Yuan et al., 2023). This heterogeneity may indicate a complex suite of climatic processes that affect precipitation isotopes in the IPWP (Konecky et al., 2016, 2019). However, a PCA of all IPWP water isotope records (excluding the Towuti n-acid record to avoid overly-weighting Lake Towuti in the mean and PCA), with at least three age controls during the deglaciation, reveals that 65% of the variance in all  $\delta^2 H_{wax}$  and  $\delta^{18} O_{speleo}$  records can be explained by the first principal component (PC1). The mean of the records is similar to PC1 and shows a clear shift from more <sup>2</sup>H-enriched to more <sup>2</sup>H-depleted precipitation centered at ~12.3 ka in most of the records, as detected by changepoint analysis (Fig. 7C; Table 1). These findings are further supported by a shift in a Sumatran speleothem record at ~12.5 ka (Wurtzel et al., 2018), though the record was too short to include in the PCA. A PCA of only the  $\delta^2 H_{wax}$  records (excluding the  $\delta^{18} O_{speleo}$  records) results in PC1 with a nearly identical structure as when the speleothem records are included (Figure A5), though the first principal component only explains 48% of the variance in the  $\delta^2 H_{\text{wax}}$  records. Change point analysis of individual records also indicates an earlier shift around ~14.5 ka, during Heinrich Stadial 1, in four of the records in addition to the shift at  $\sim$ 12.3 ka (Fig. 10).

The timing of the shift in precipitation isotope records, at 12.3 ka (Fig. 7) coincides with the deglacial shift indicated in runoff and sea surface salinity proxies (Fig. 10). The agreement between precipitation isotope records and other precipitation amount proxies may indicate that  $\delta^2 H_{wax}$  and speleothem  $\delta^{18} O_{speleo}$  respond strongly to, and may be reliable proxies for, precipitation amount on orbital timescales in the IPWP. Additionally, the timing of the shift in precipitation isotope records coincides with flooding of the Sunda and Sahul shelves (Pico et al., 2020). Existing studies have observed the similar timing of shelf inundation and precipitation amount, as inferred from  $\delta^{18} O_{speleo}$  records (Krause et al., 2019). However,  $\delta^2 H_{wax}$  and speleothem  $\delta^{18} O_{speleo}$  records may also be affected by changes in moisture source, cloud type, convergence/divergence, and/or moisture transport, many of which also change with Sunda and Sahul shelf inundation (Du et al., 2021; Konecky et al., 2016, 2019).

Table 1

All IPWP records included in compilation. Deglacial changepoints as detected by detected using the "EnvCpt" package in R (Killick et al., 2021).

Paper	Proxy	Location	Core/Cave	Deglacial changepoint (ka)	Age uncertainty at changepoint (ka)
Mohtadi et al. (2011)	Ln(Ti/Ca)	South of East Java	GeoB10053-7	13.0	0.4
Hollstein et al. (2018)	Ln(Ti/Ca)	North of New Guinea	GeoB17419-1	9.1	0.9
Fraser et al. (2014)	Log(Fe/Ca)	Offshore Mindanao	MD06-3075	12.6	0.9
Costa et al. (2015)	Ti	Lake Towuti	TOW9B	14.7	0.9
Mohtadi et al. (2014)	$\delta^{18}O_{calcite}$	Offshore Sumatra	SO189-2_119 KL	14.7	0.7
Mohtadi et al. (2014)	$\delta^{18}O_{calcite}$	Offshore Sumatra	SO189-2_039 KL	15.2 and 11.5	0.2 and 0.2
Sarnthein et al. (2011) and Xu et al. (2008)	$\delta^{18}O_{calcite}$	Timor Sea	MD01-2378	Not detected	NA
Schröder et al. (2018)	$\delta^{18}O_{calcite}$	Makassar Strait	GIK18526-3	10.9	0.4
Schröder et al. (2018)	$\delta^{18}O_{calcite}$	Makassar Strait	GIK18519-2	Not detected	NA
Schröder et al. (2018)	$\delta^{18}O_{calcite}$	Makassar Strait	GIK18522-3	11.8	0.2
Fan et al. (2018)	$\delta^{18}O_{calcite}$	Makassar Strait	MD98-2178	11.4	0.3
Stott et al. (2007)	$\delta^{18}O_{calcite}$	Offshore West Papua	MD98-2176	Not detected	NA
Stott et al. (2002)	$\delta^{18}O_{calcite}$	Offshore Mindanao	MD98-2181	12.9	0.2
Gibbons et al. (2014)	$\delta^{18}O_{calcite}$	Savu Sea	GeoB10069-3	12.4	0.5
Levi et al. (2007)	δ <sup>18</sup> O <sub>calcite</sub>	Offshore Flores	MD98-2165	12.7	0.4
Visser et al. (2003)	δ <sup>18</sup> O <sub>calcite</sub>	Makassar Strait	MD98-2162	10.8	0.6
Ruan et al. (2019)	C <sub>31</sub> <i>n</i> -alkane δ <sup>2</sup> H	Offshore Java	GeoB10053-7	13.4	0.3
This study	$C_{31}$ <i>n</i> -alkane $\delta^2$ H	Lake Towuti	TOW9B	9.5	0.6
Konecky et al. (2016)	C28 <i>n</i> -acid $\delta^2$ H	Lake Towuti	TOW9B	11.3	0.4
This study	$C_{31}$ n-alkane $\delta^2$ H	Lake Matano	IDLE-MAT10-2B	12.0	2.2
Wicaksono et al. (2017)	C28 n-acid δ <sup>2</sup> H	Mandar Bay	SO18515	10.8	0.4
Niedermeyer et al. (2014)	C30 n-acid δ <sup>2</sup> H	Offshore Sumatra	SO189-144 KL	Not detected	NA
Krause et al. (2019)	Speleothem δ <sup>18</sup> Ο	Sulawesi	Gempa Bumi Cave	14.4 and 12.4	0.1and 0.2
Partin et al. (2007)	Speleothem δ <sup>18</sup> Ο	Borneo	Snail Shell and Bukit Assam caves	14.6 and 12.3	0.1 and 0.1
Ayliffe et al. (2013)	Speleothem δ <sup>18</sup> Ο	Flores	Liang Luar Cave	11.5	0.1
Yuan et al. (2023)	Speleothem δ <sup>18</sup> Ο	Sulawesi	Southwest Sulawesi caves	14.7 and 10.5	0.2 and 0.2
Dubois et al. (2014)	C30 n-acid $\delta^{13}$ C	Offshore Borneo	91GGC	Not detected	NA
Niedermeyer et al. (2014)	C30 n-acid $\delta^{13}$ C	Offshore Sumatra	SO189-144 KL	Not detected	NA
Dubois et al. (2014)	C30 n-acid $\delta^{13}$ C	Offshore Java	GeoB10069-3	19.8	0.7
Wicaksono et al. (2017)	C28 n-acid $\delta^{13}$ C	Mandar Bay	SO18515	19.8	0.5
Ruan et al. (2019)	$C_{31}$ <i>n</i> -alkane $\delta^{13}C$	Offshore Java	GeoB10053-7	19.5	0.5
This study	$C_{31}$ <i>n</i> -alkane $\delta^{13}C$	Lake Towuti	TOW9B	22.3	0.8
Konecky et al. (2016)	C28 n-acid $\delta^{13}$ C	Lake Towuti	TOW9B	17.2	0.6
This study	$C_{31}$ <i>n</i> -alkane $\delta^{13}C$	Lake Matano	IDLE-MAT10-2B	20.8	1.4
Wicaksono et al. (2015)	C28 n-acid δ <sup>13</sup> C	Lake Matano	IDLE-MAT10-2B	Not detected	NA

### 5.3. Leaf wax isotope records of vegetation change

 $\delta^{13}C_{wax}$  records from the IPWP share common trends (Dubois et al., 2014; Niedermeyer et al., 2014; Ruan et al., 2019; Russell et al., 2014; Wicaksono et al., 2015, 2017; Windler et al., 2019; Wurster et al., 2019). A PCA of all marine and lacustrine IPWP  $\delta^{13}C_{wax}$  records with at least three age controls during the deglaciation (excluding the Towuti and Matano n-acid records to avoid overly weighting these sites) results in a PC1 that explains 96% of the variance in all records (Fig. 8). All records show  $^{13}C$ -enrichment during the LGM relative to  $^{13}C$ -depletion during the Holocene, except for 91GGC from offshore eastern Borneo (Dubois et al., 2014) and SO189-144 KL from offshore Sumatra (Niedermeyer et al., 2014). The  $^{13}C$ -enrichment at the LGM ranges from 2 to 9% heavier than the mean  $\delta^{13}C_{wax}$  between 10 and 8 ka in each record, excluding 91GGC and SO189-144 KL (Table A1; Fig. 8B). Changepoint analysis reveals that the records begin to become more  $^{13}C$ -depleted between 22.3 and 17.2 ka with an average of 19.9 ka (Table 1; Fig. 10).

The amplitudes of change suggest variable changes in vegetation, with the largest amplitudes signaling substantial decreases in the abundance of plants using the  $C_4$  photosynthetic pathway during the deglaciation. Averaging all  $\delta^{13}C_{wax}$  records from the IPWP results in a  $\sim$ 4% shift, from -28 to -32%, from the LGM to the Holocene (Fig. 8C).

The largest shifts in  $\delta^{13}C_{wax}$  occurred at the sites with the highest modern mean annual precipitation (Fig. 9B); however, modern mean annual precipitation is not significantly correlated with the magnitude of the LGM-Holocene shift in  $\delta^{13}C_{wax}$  (R² = 0.19; p>0.05).

The  $\delta^{13}C_{wax}$  shift in the records could be explained by changes in water stress and/or by changes in the ratio of  $C_3$  to  $C_4$  plants. Fractionation of carbon is dependent on plant moisture stress, with wetter conditions leading to more efficient leaf-gas exchange and more depleted  $\delta^{13}C$  values (Diefendorf et al., 2010). A shift in  $\delta^{13}C_{wax}$  can also be caused by a shift in the ratio of  $C_3$  to  $C_4$  plants because of their distinct isotopic compositions (Figure A2). Many, if not most, of the records in the IPWP likely record both decreasing moisture stress and increasing  $C_3$  plants during the deglaciation, given palynological evidence for decreasing grass abundance in many parts of the IPWP (Dubois et al., 2014; Hamilton et al., 2019; Hope, 2001; Ruan et al., 2019; van der Kaars et al., 2010).

The effects of water stress vs. changes in plant photosynthetic pathway can be difficult to discern, and we can only definitively diagnose increasing  $C_3$  plants from  $\delta^{13}C_{wax}$  when there is a large shift from values within the modern  $C_4$  range to values within the  $C_3$  range beyond that expected from water stress alone (Figure A2). To assess the factors influencing  $\delta^{13}C_{wax}$ , we calculated the percent  $C_3$  using a mixing model

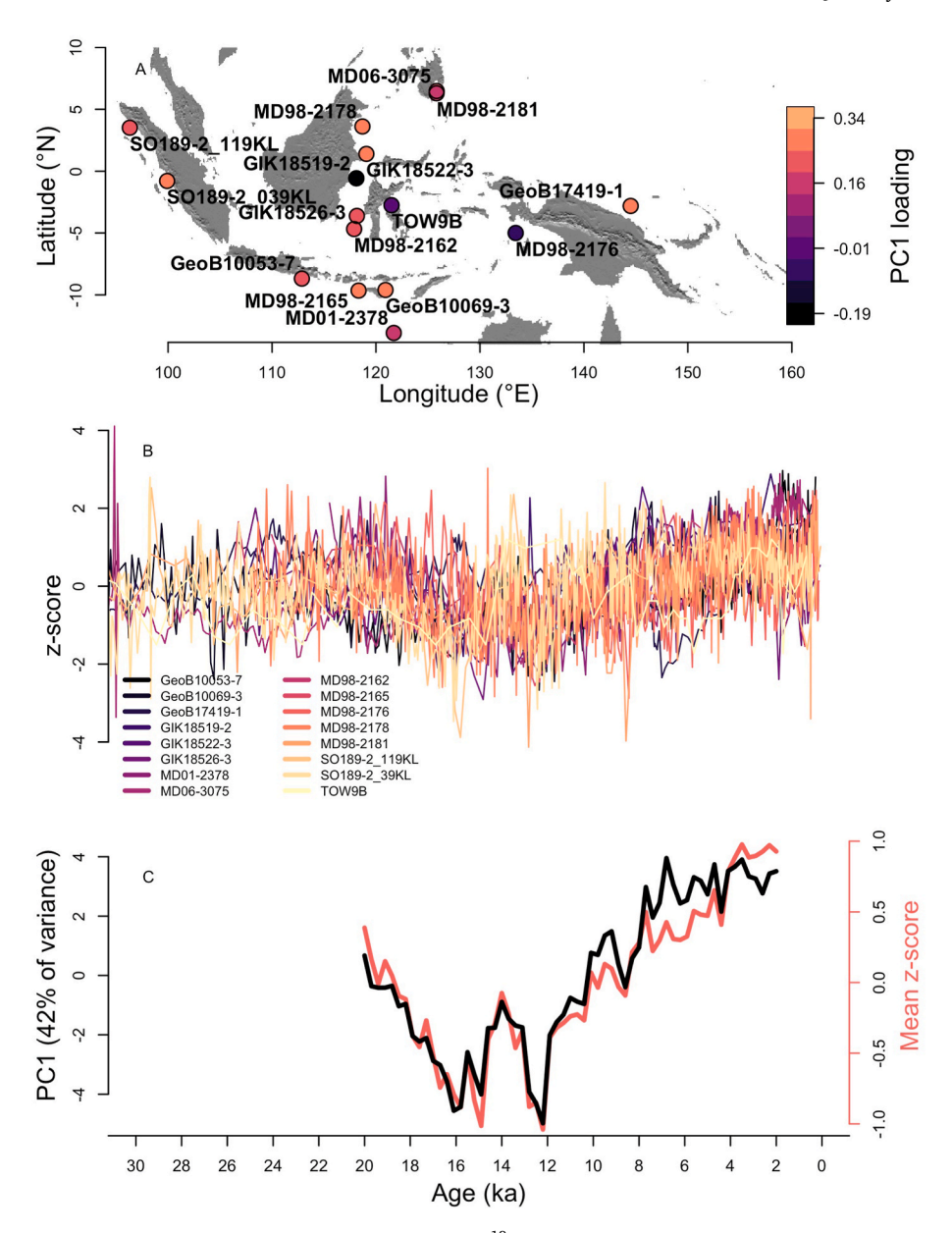


Fig. 6. (A) Map of the location of all the sites included in the synthesis of IPWP  $\delta^{18}O_{sw}$  and runoff records with at least three age controls between 20 and 12 ka (Costa et al., 2015; Fan et al., 2018; Fraser et al., 2014; Gibbons et al., 2014; Hollstein et al., 2018; Levi et al., 2007; Mohtadi et al., 2011, 2014; Rosenthal et al., 2003; Sarnthein et al., 2011; Schröder et al., 2018; Stott et al., 2002, 2007; Visser et al., 2003; Xu et al., 2008), colored by their loading on PC1. (B) Z-scores of all the  $\delta^{18}O_{sw}$  and runoff records. (C) The mean z-score (orange) and PC1 (black) of the records.

that does not take into account moisture stress (Konecky et al., 2016). The individual records show that the two sites with highest modern percent (>78%) C<sub>3</sub> experienced the greatest change in fraction C<sub>3</sub> over the deglaciation (Fig. 9). These sites - Lake Towuti and Lake Matano shift from less than 30% C<sub>3</sub> plants at the LGM to over 70% C3 plants during the Holocene, suggesting a reduction in the extent of the closed-canopy rainforests during the LGM. GeoB10053-7 from offshore Java also shows a large magnitude shift from below 50% C<sub>3</sub> at the LGM to over 68% at modern. Of note, the three sites with highest modern fraction C<sub>3</sub> are also the three sites with records based on isotopic analyses of *n*-alkanes, rather than *n*-acids. However, the comparison between alkanes and acids at Lake Towuti and Lake Matano indicates that the use of *n*-acids can either amplify or dampen the magnitude of the shift in  $\delta^{13}\text{C}$  compared to alkanes (Fig. 5). The two sites with between 50 and 67% C3 in the most modern samples (91GGC offshore Borneo and SO189-144 KL from offshore Sumatra) do not show a trend from the LGM to the Holocene, hovering around 60% C<sub>3</sub> plants throughout the deglaciation. The lack of trend at the Borneo site is surprising, as a nearby bat guano  $\delta^{13} C$  record from southern Borneo suggested savannah expansion during the LGM (Wurster et al., 2019). The modern reconstructed 66%  $C_3$  plants at Borneo also does not reflect the tropical lowland and montane rainforest present today (Dubois et al., 2014), which may point to remote aeolian contributions of n-acids to these sediments. The two sites with less than 30%  $C_3$  in their most modern measurements (SO18515 in Mandar Bay and GeoB10069-3 offshore Java) show a clear change to more negative values during the deglaciation, but the magnitude of change is much smaller than the sites that are rainforests today.

## 5.4. Forcings of precipitation change

Precipitation amount is challenging to reconstruct from proxy archives. Precipitation isotopes, vegetation change, clastic sediment fluxes, and a variety of other proxies have been used to estimate

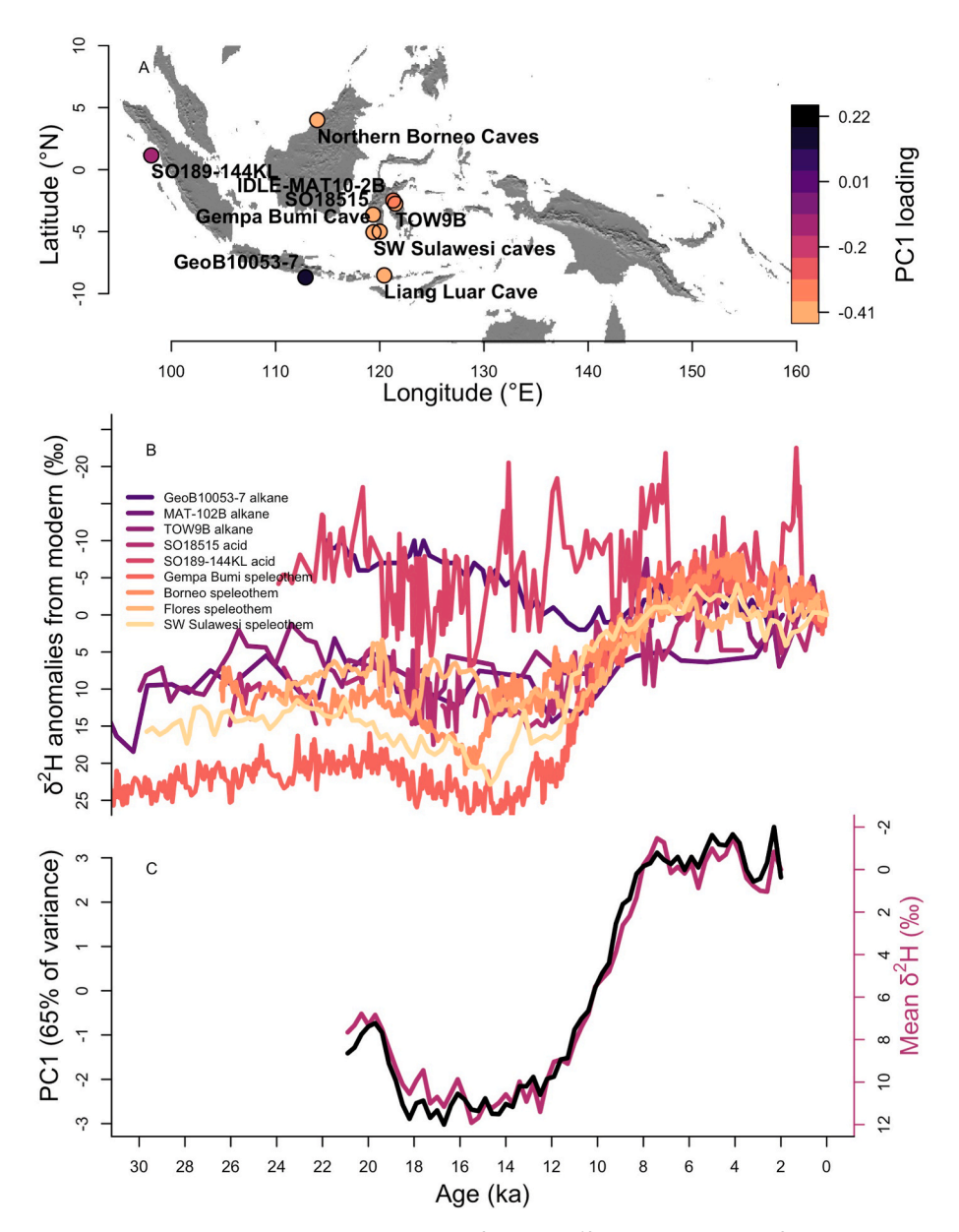


Fig. 7. (A) Map of the location of all the sites included in the synthesis of IPWP  $\delta^2 H_{wax}$  and  $\delta^{18} O_{speleo}$  (converted to  $\delta^2 H$ -space using the global meteoric water line) records with at least three age controls between 20 and 12 ka (Ayliffe et al., 2013; Griffiths et al., 2009; Konecky et al., 2016; Krause et al., 2019; Niedermeyer et al., 2014; Partin et al., 2007; Ruan et al., 2019; Wicaksono et al., 2017; Yuan et al., 2023), colored by their loading on PC1. The Towuti acid record is excluded to avoid overly-weighting Lake Towuti in the mean and PCA. (B) The  $\delta^2 H$  anomalies from modern. (C) The mean  $\delta^2 H$  anomaly from modern (pink) and PC1 (black) of the records.

precipitation amounts in the past, but all of these proxies are influenced by multiple climatic, ecologic, and/or geologic processes. We rely on runoff records and  $\delta^{18}O_{sw}$  records as more direct indicators of precipitation change, which point to increasing precipitation amount during the Younger Dryas in 8 records, although an initial moisture increase is detected during Heinrich Stadial 1 in three records (Fig. 10). The spread in timing may reflect an increase in moisture during both Heinrich Stadial 1 and the Younger Dryas, potentially in different parts of the IPWP, but also highlights the continued difficulty in reconstructing precipitation amount.

PC1 of precipitation isotopes shifts at  $\sim$ 12.3 ka, which could be further evidence for increasing precipitation amount during the last deglaciation. However, there are many controls on the isotopic composition of precipitation in the IPWP. A comparison of precipitation amount and its isotopic composition during the LGM and the Early Holocene in the iTRACE simulations indicated variable relationships

between precipitation amount and isotopic composition, including regions with both negative (as predicted by the amount effect) and positive (opposite the amount effect) correlations (Du et al., 2021). The latter occurred at some sites near exposed shelf areas, potentially due to shifts in moisture source. The iTRACE experiment simulated a SW-NE dipole pattern of  $\delta^2 H_{precip}$  anomalies over the IPWP, with the eastern Indian Ocean showing more <sup>2</sup>H-enrichment during the LGM relative to the Holocene, and <sup>2</sup>H-depletion at the LGM relative to the Holocene in Borneo, Sulawesi, and Papua (Du et al., 2021). The enrichment during the LGM was attributed to increased divergence and subsidence related to shelf exposure, which favor rain re-evaporation that removes lighter isotopes over the eastern Indian Ocean (Du et al., 2021). Although the δ<sup>2</sup>H<sub>precip</sub> anomaly showed a dipole structure, the first principal component of precipitation isotope records revealed more ubiquitous <sup>2</sup>H-enrichment during the LGM relative to the Holocene across the Maritime Continent (Du et al., 2021).

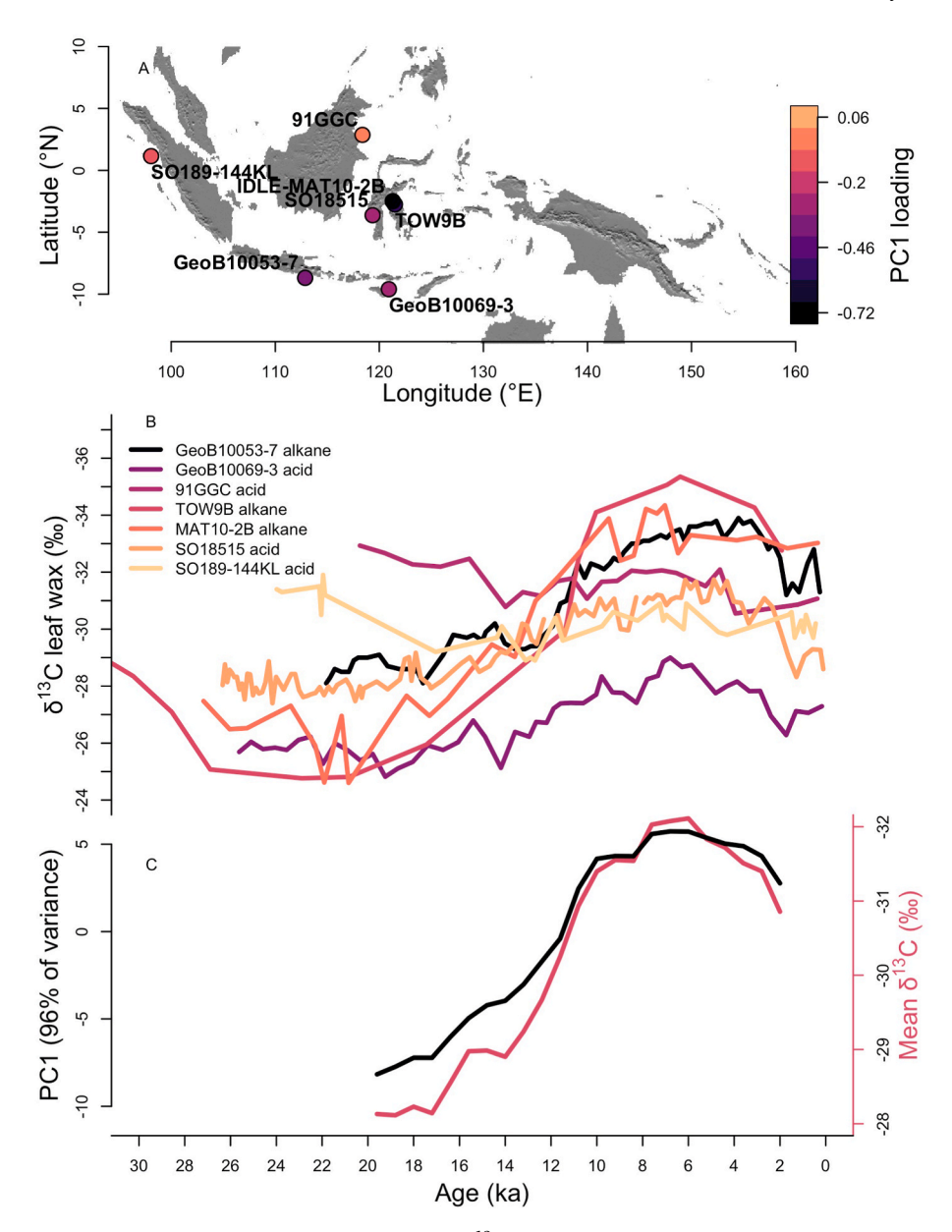


Fig. 8. (A) Map of the location of all the sites included in the synthesis of IPWP  $\delta^{13}C_{wax}$  records with at least three age controls between 20 and 12 ka (Dubois et al., 2014; Niedermeyer et al., 2014; Ruan et al., 2019; Wicaksono et al., 2017), colored by their loading on PC1. The Towuti and Matano acid records are excluded to avoid overly-weighting Lake Towuti and Lake Matano in the mean and PCA. (B) The measured  $\delta^{13}C_{wax}$  of all the records. (C) The mean  $\delta^{13}C_{wax}$  (pink) and PC1 (black) of the records.

Despite the varied influences on runoff, salinity, and precipitation isotope proxies, when taken together, the synchrony of deglacial shifts in runoff,  $\delta^{18}O_{sw}$ , and precipitation isotope records provide support for increasing precipitation over the IPWP at ~12.3 ka. The shift from a drier LGM to a wetter Holocene is supported by a variety of other records, though not all agree with the timing of this change. A compilation of coral, marine sediment, lake sediment, speleothem, and charcoal was used to infer increasing precipitation in Indonesia starting at ~17 ka (Reeves et al., 2013). This timing was largely based on increasing lowland rainforest pollen detected in cores from Java and Sumatra (Reeves et al., 2013); however, rainforest expansion may be influenced by a variety of factors including atmospheric CO2 concentrations (Kimbrough et al., 2023) and precipitation seasonality (Dubois et al., 2014) rather than rainfall amount alone. On Sulawesi there is additional proxy evidence of increasing moisture during the deglaciation, including a lake level reconstruction from Lake Towuti (Vogel et al., 2015) and a charcoal record from Lake Lantoa (Hamilton et al., 2019). However, the timing of rising lake levels is difficult to determine, and fire frequency is influenced by a variety of climatic and ecological processes.

The timing of the shift in our syntheses, at ~12.3 ka, coincides with the timing of the flooding of the majority of the Sunda and Sahul shelves, when sea levels rose above 50 m below modern (Du et al., 2021; Lambeck et al., 2014) at ~12.5 ka (Hanebuth et al., 2000, 2011). Climate models suggest that the exposure of the continental shelves in the IPWP during the LGM induced anomalous southeasterlies off the coast of Java and Sumatra, which caused increased upwelling and cooling (DiNezio et al., 2018). Cooling in the eastern Indian Ocean decreased the zonal SST gradient and weakened Indian Ocean Walker Circulation, leading to atmospheric divergence and decreased precipitation over the Maritime Continent at the LGM compared to the Holocene (DiNezio et al., 2016, 2018; DiNezio and Tierney, 2013; Du et al., 2021). In the iTRACE simulation, the flooding of the Northwestern Australian Shelf at 14 ka, when sea level rose above 65 m below modern, caused large-scale precipitation change over the tropical Indian Ocean (Du et al., 2021). In

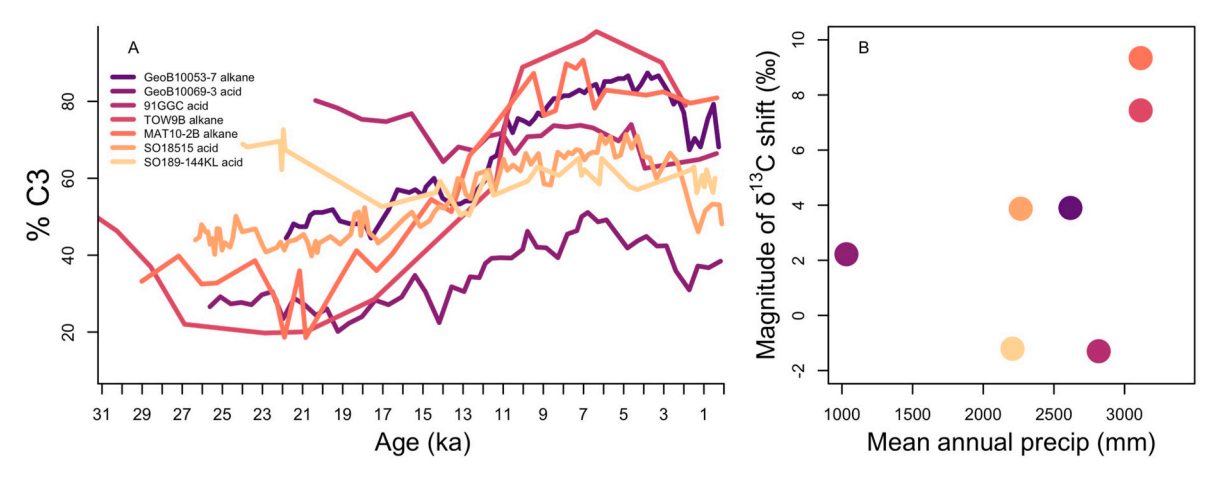


Fig. 9. A) Percent  $C_3$  estimated from an end-member mixing model based on all marine and lacustrine leaf wax  $\delta^{13}C_{wax}$  records from the IPWP (excluding the Towuti and Matano acid records). B) Mean annual precipitation from 1992 to 2022 from GPCP data with 1° resolution (Adler et al., 2018) and the magnitude of deglacial shift in  $\delta^{13}C_{wax}$  calculated by subtracting the mean between 10 and 8 ka from the mean between 22 and 20 ka.

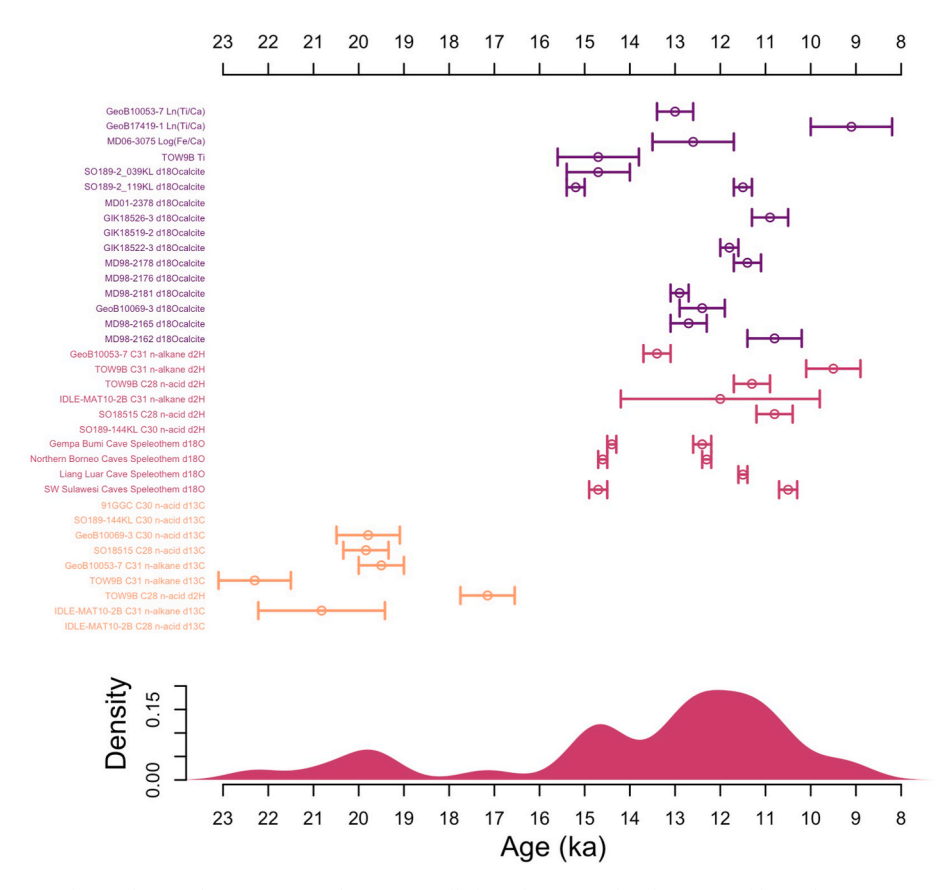


Fig. 10. Deglacial changepoints detected using the "EnvCpt" package in R (Killick et al., 2021), also shown in Table 1. The 1-sigma uncertainty was determined by recalibrating the radiocarbon dates to IntCal20 and determining the uncertainty of the age-models using Bacon (Blaauw and Christen, 2011). A probability density function of the changepoints from all of the hydroclimate and vegetation proxies is shown in the bottom panel.

iTRACE, the Northwestern Australian Shelf was inundated at 14 ka, which is the same time sea level was expected to be 65 m below modern in the Sunda core region (Hanebuth et al., 2011; Lambeck et al., 2014), but there are no estimates of the timing of this flooding from the Northwestern Australian Shelf itself (Lewis et al., 2013). The simulation also indicates increased precipitation over the Maritime Continent with the flooding of the majority of the Sunda and Sahul shelves at 12 ka, but the simulated increase in rainfall at this time does not cover as broad of a spatial scale as the shelf inundation at 14 ka (Du et al., 2021).

Our reconstructed timing of increased precipitation reflected in

runoff, salinity, and precipitation isotope records at  $\sim 12.3$  ka, suggests the flooding of the majority of the Sunda and Sahul shelves at 12.5 ka caused more significant precipitation increase over the Maritime Continent than the earlier flooding of the NW Australian shelf when sea level rose above 65 m below modern and caused the large-scale tropical Indian Ocean dipole. Seven records do indicate increasing precipitation during Heinrich Stadial 1 (Fig. 10), when the NW Australian Shelf may have become inundated. Further work is needed to investigate interactions between flooding of different parts of the shelves and climate boundary conditions to unravel the causes of these rainfall changes.

### 5.5. Causes of vegetation change

Support for decreasing  $C_4$  plants – most notably tropical grasses and sedges – during the deglaciation is apparent in many palynogical records from the IPWP. Decreasing *Cyperaceae*, which is mostly  $C_4$  in the tropics (Bruhl and Wilson, 2007), and *Poaceae* was observed at Lake Lantoa and Wanda Swamp in Sulawesi, offshore Java, and offshore Sumatra (Dubois et al., 2014; Hamilton et al., 2019; Hope, 2001; Ruan et al., 2019; van der Kaars et al., 2010). Given the range in the  $\delta^{13}$ C of  $C_3$  and  $C_4$  plants it is difficult to quantify the extent of  $C_4$  expansion during the LGM. Overall the data are consistent with retraction of  $C_4$  sedges and grasses during the deglaciation.

Despite this evidence, not all of the change in  $\delta^{13}C_{wax}$  may be attributed to increasing C<sub>3</sub> plants during the deglaciation. A shift from more <sup>13</sup>C-enrichment at the LGM to more <sup>13</sup>C-depletion during the Holocene could be controlled by water-stress related to rainfall, humidity, or temperature, CO2 concentration, or precipitation amount. Increased temperature would cause a shift to more <sup>13</sup>C-enriched values after the deglaciation (Pagani et al., 1999), suggesting temperature is not the primary control on the  $\delta^{13}C_{wax}\,\text{records}$  in the IPWP. As plants are able to fractionate carbon isotopes more effectively at higher CO2 concentrations, rising CO<sub>2</sub> could explain the direction of change during the deglaciation. In northwest Africa, for instance, the composition of savannah ecosystems is influenced by atmospheric CO2 concentrations (Kuechler et al., 2013; O'Mara et al., 2022). However, changepoint analysis of our IPWP data indicates  $\delta^{13}C_{wax}$  begins to increase at  $\sim 19.9$ ka (Table 1), prior to the deglacial CO2 increase (Marcott et al., 2014) at 17.5 ka. The earliest that any runoff or salinity record indicates increasing precipitation is 15.2 ka in SO189-2\_039 KL, and the largest changes appear to occur at about 12.3 ka, well after the shift in  $\delta^{13}C_{\text{wax}}$ . Although increasing precipitation likely contributes to the expansion of rainforests, the initial transition in  $\delta^{13}C_{\text{wax}}$  cannot be explained by annual precipitation amount alone. Although the increasing CO2 concentrations and increasing annual precipitation likely contributed to changes in δ<sup>13</sup>C<sub>wax</sub> through increasing carbon use efficiency and decreasing water stress, the initial shift in  $\delta^{13}C_{wax}$  may be primarily related to other factors.

Dubois et al. (2014) showed, in the present day,  $\delta^{13}C_{wax}$  is more strongly correlated to the severity of the dry season than to mean annual rainfall. Year-round high precipitation rates are required to maintain closed-canopy rainforest (Dubois et al., 2014), and a drier and/or longer dry season can reduce the extent of closed canopy forests and favor  $C_4$  grass expansion (Dubois et al., 2014; Jiang et al., 2019). Although precipitation seasonality is very difficult to reconstruct, some regional records have inferred increased seasonality at the LGM compared to the Holocene in the Maritime Continent based on  $\delta^{13}C_{wax}$ , with longer, drier dry seasons and shorter, wetter wet seasons on Sumba and Palawan (Dubois et al., 2014; Ruan et al., 2019).

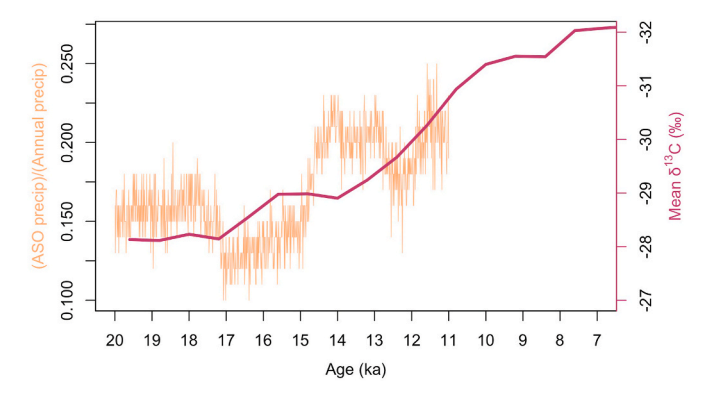


Fig. 11. The transient evolution of the ASO fraction of annual precipitation from iTRACE (orange) and the mean  $\delta^{13}C_{wax}$  of all IPWP records (pink).

The iTRACE simulation indicates increasing dry season precipitation during the deglaciation (Fig. 11). Although dry season rainfall in the simulation begins to increase at 17.2 ka, rather than 19.9 ka as indicated in the leaf wax records, the shift precedes the shelf-flooding events at 14 and 12 ka that lead to increased annual precipitation (Fig. 11; Du et al., 2021). This suggests that controls on precipitation seasonality and mean annual amount may diverge, so if dry season precipitation increased during the deglaciation the change could favor  $C_3$  plant expansion before substantial changes occurred in mean annual precipitation. An increase in JJA precipitation relative to DJF precipitation in the entire Sunda region (3° S–1° N, 100–104° E) was also observed in the TRACE simulation (Hällberg et al., 2022). The JJA/DJF ratio gradually begins to increase at the beginning of the simulation, at 20 ka, and rapidly increases at 14.7 ka at the beginning of the Bølling-Allerød (Hällberg et al., 2022).

Although we have no direct proxy evidence to support the simulated changes in precipitation seasonality, it is difficult to explain the early transitions in  $\delta^{13}C_{wax}$  relative to changes in rainfall amount, temperature, and atmospheric  $\text{CO}_2$  concentrations. We infer that the transition in  $\delta^{13}C_{wax}$  may have been initiated by an increase in dry season precipitation. Continued increases in dry season precipitation, as well as mean annual precipitation and atmospheric  $\text{CO}_2$ , likely contributed to the subsequent expansion of closed-canopy rainforests and C3 plants later during the deglaciation.

### 6. Conclusions

As sea level rose during the last deglaciation, runoff and salinity proxies indicate increasing precipitation over the Maritime Continent as a result of the flooding of large areas of the Sunda and Sahul shelves at  $\sim\!12.3$  ka. The inundation of the shelves led to a large-scale depletion in the isotopic composition of  $\delta^2H_{wax}$  and  $\delta^{18}O_{speleo}$  at  $\sim\!12.3$  ka in response to increasing precipitation amount and convergence.  $\delta^{13}C_{wax}$  begins to decrease at  $\sim\!19.9$  ka, well before CO<sub>2</sub> and annual precipitation begin to increase, pointing to a change in the seasonality of the precipitation as the initiator of changing  $\delta^{13}C_{wax}$  through a shift to more C<sub>3</sub> plants. The increase in CO<sub>2</sub> and annual precipitation continue to shift  $\delta^{13}C_{wax}$  to more negative values throughout the deglaciation.

### **Declaration of competing interest**

The authors declare that they have no known competing financial interests or personal relationships that could have appeared to influence the work reported in this paper.

## Data availability

The Towuti and Matano leaf wax records are available at: https://www.ncei.noaa.gov/access/paleo-search/study/39564

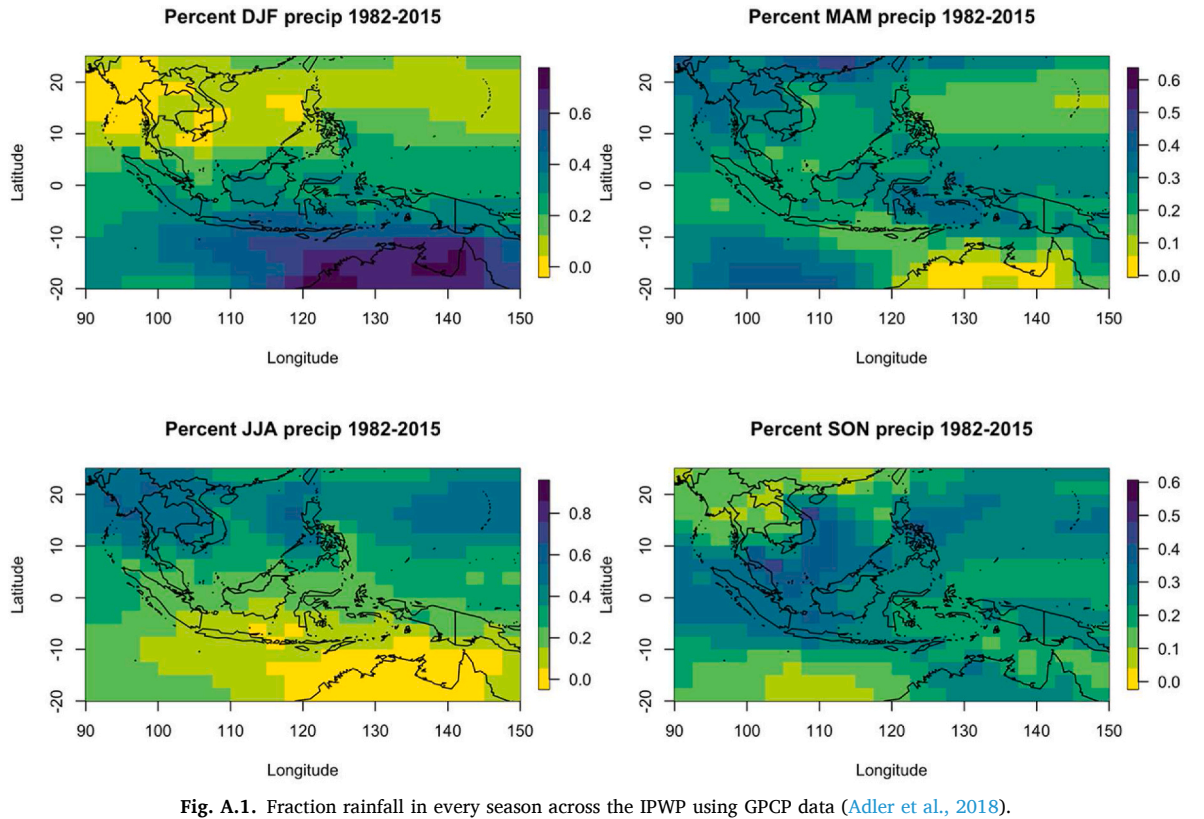
### Acknowledgements

We would like to thank Alexander Wilk for his careful and diligent lab assistance with processing some of the Lake Matano samples, and Ewerton Santos for his work maintaining the GC-FID and GC-IRMS. This material is based on work supported by National Science Foundation Grant EAR-2102856. The authors thank Gerald Tamuntuan, Satrio Wicaksono, Nigel Wattrus, and PT Vale Indonesia for field assistance. The authors acknowledge assistance and permission for this work from the Indonesian Ministry of Research and Technology (RISTEK).

### Appendix

Table A.1  $\delta^{13}C_{wax}$  records included in compilation. Mean annual precipitation from 1992 to 2022 from GPCP data with 1° resolution (Adler et al., 2018). Magnitude of deglacial shift in  $\delta^{13}C_{wax}$  calculated by subtracting the mean between 10 and 8 ka from the mean between 22 and 20 ka.

Paper	Proxy	Location	Core	Mean annual precipitation (mm)	Magnitude of shift (‰)
Dubois et al. (2014)	C30 n-acid	Offshore Borneo	91GGC	2817	-1.3
Niedermeyer et al. (2014)	C30 n-acid	Offshore Sumatra	SO189-144 KL	2207	-1.21
Dubois et al. (2014)	C30 n-acid	Offshore Java	GeoB10069-3	1032	2.22
Wicaksono et al. (2017)	C28 n-acid	Mandar Bay	SO18515	2265	3.87
Ruan et al. (2019)	C <sub>31</sub> n-alkane	Offshore Java	GeoB10053-7	2617	3.9
This study	$C_{31}$ n-alkane	Lake Towuti	TOW9B	3114	7.44
This study	C <sub>31</sub> n-alkane	Lake Matano	IDLE-MAT10-2B	3114	9.34



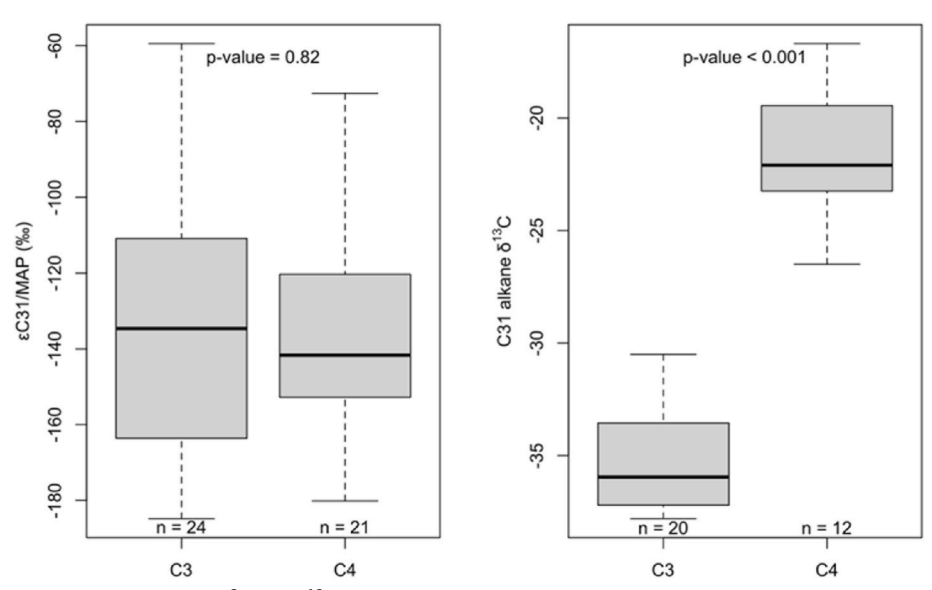


Fig. A.2. Boxplots of the apparent fractionation of  $\delta^2 H$  and  $\delta^{13} C$  of  $C_{31}$  *n*-alkanes by all C3 and C4 plants included in the Sachse et al. (2012) compilation from between 30°S and 30°N. A t-test reveals that the mean apparent fractionation  $^2$ H/H of C3 and C4 plants is not significantly different (p-value = 0.82), and mean  $\delta^{13}$ C is significantly different (p < 0.001).

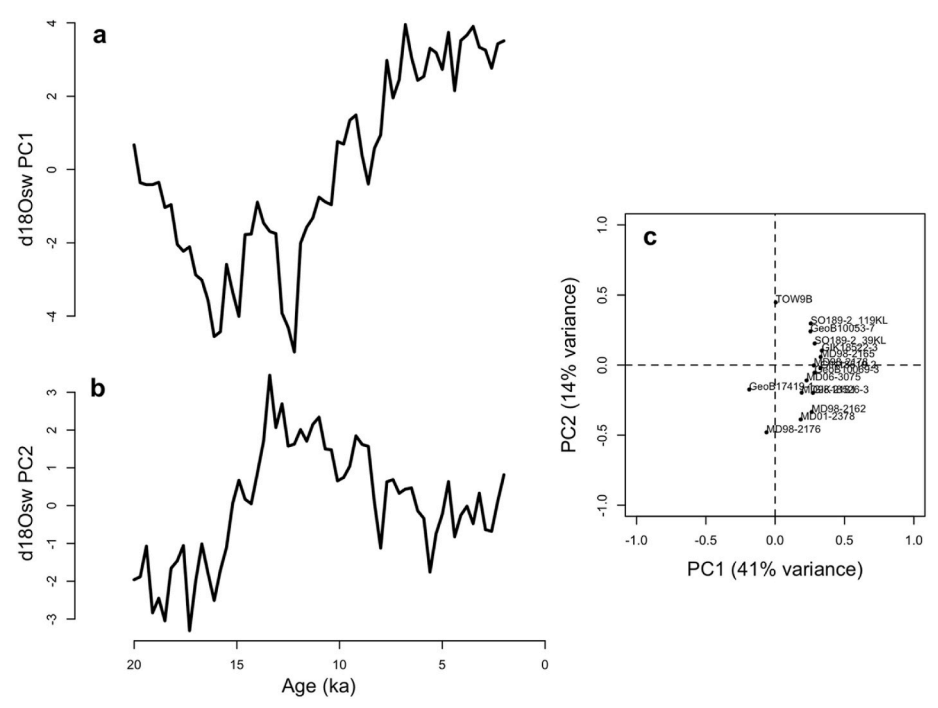


Fig. A.3. PCA of all runoff and  $\delta^{18}O_{sw}$  records from the IPWP with three age controls between 20 and 12 ka. The mean resolution of all the records is 0.3 ka, which was used as the common timestep.

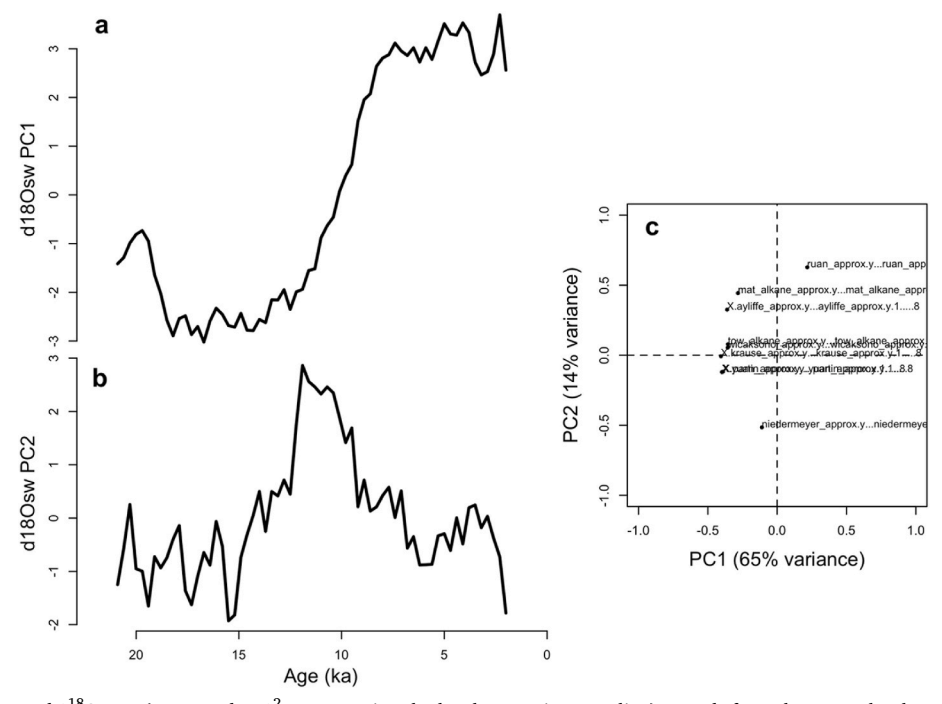


Fig. A.4. PCA of all  $\delta^2 H_{wax}$  and  $\delta^{18} O_{speleo}$  (converted to  $\delta^2 H$ -space using the local meteoric water line) records from the IPWP that have at least three age controls during the last deglaciation (excluding the Towuti acid record to avoid overly-weighting Lake Towuti in the mean and PCA). The mean resolution of all the records is 0.3 ka, which was used as the common timestep.

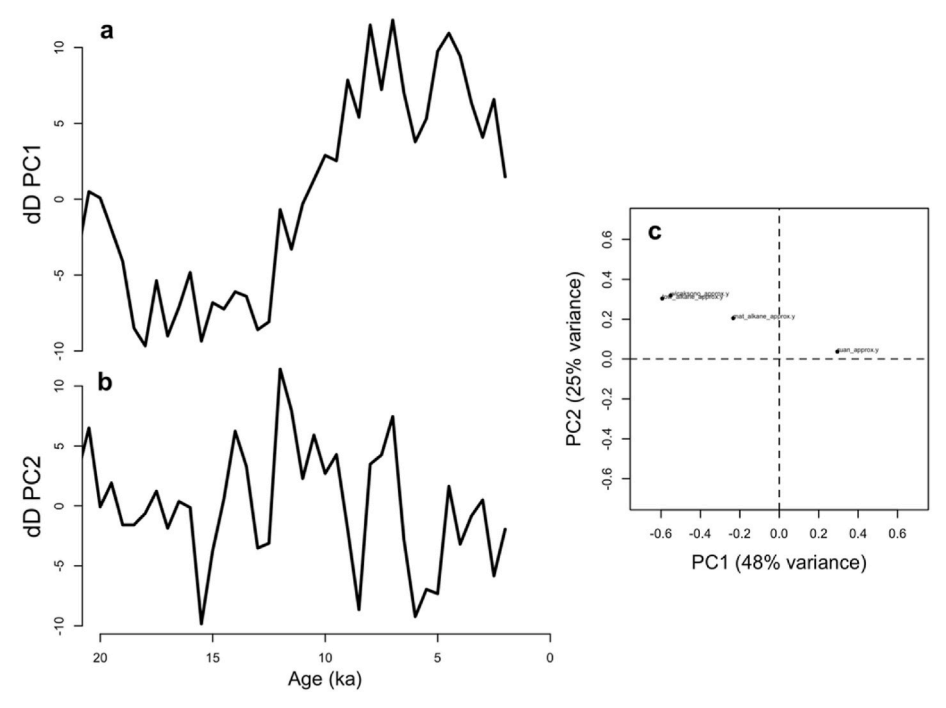


Fig. A.5. PCA of all  $\delta^2 H_{wax}$  records from the IPWP that have at least three age controls during the last deglaciation (excluding the Towuti acid record to avoid overly-weighting Lake Towuti in the mean and PCA).

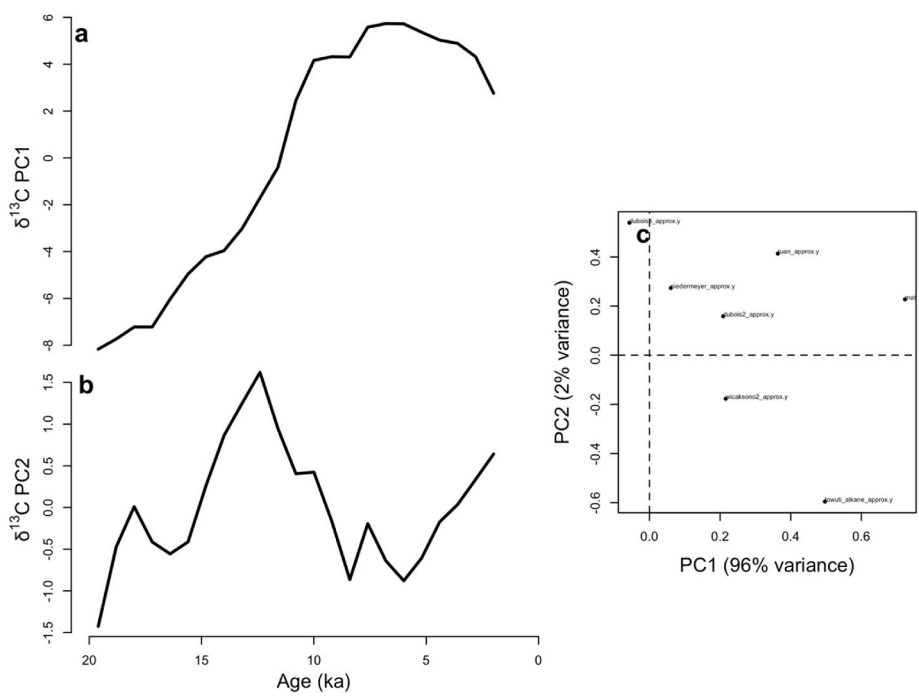


Fig. A.6. PCA of all  $\delta^{13}C_{\text{wax}}$  records from the IPWP (excluding the Matano acid record to avoid overly weighting Lake Matano in the mean and PCA). The mean resolution of all the records is 0.8 ka, which was used as the common timestep.

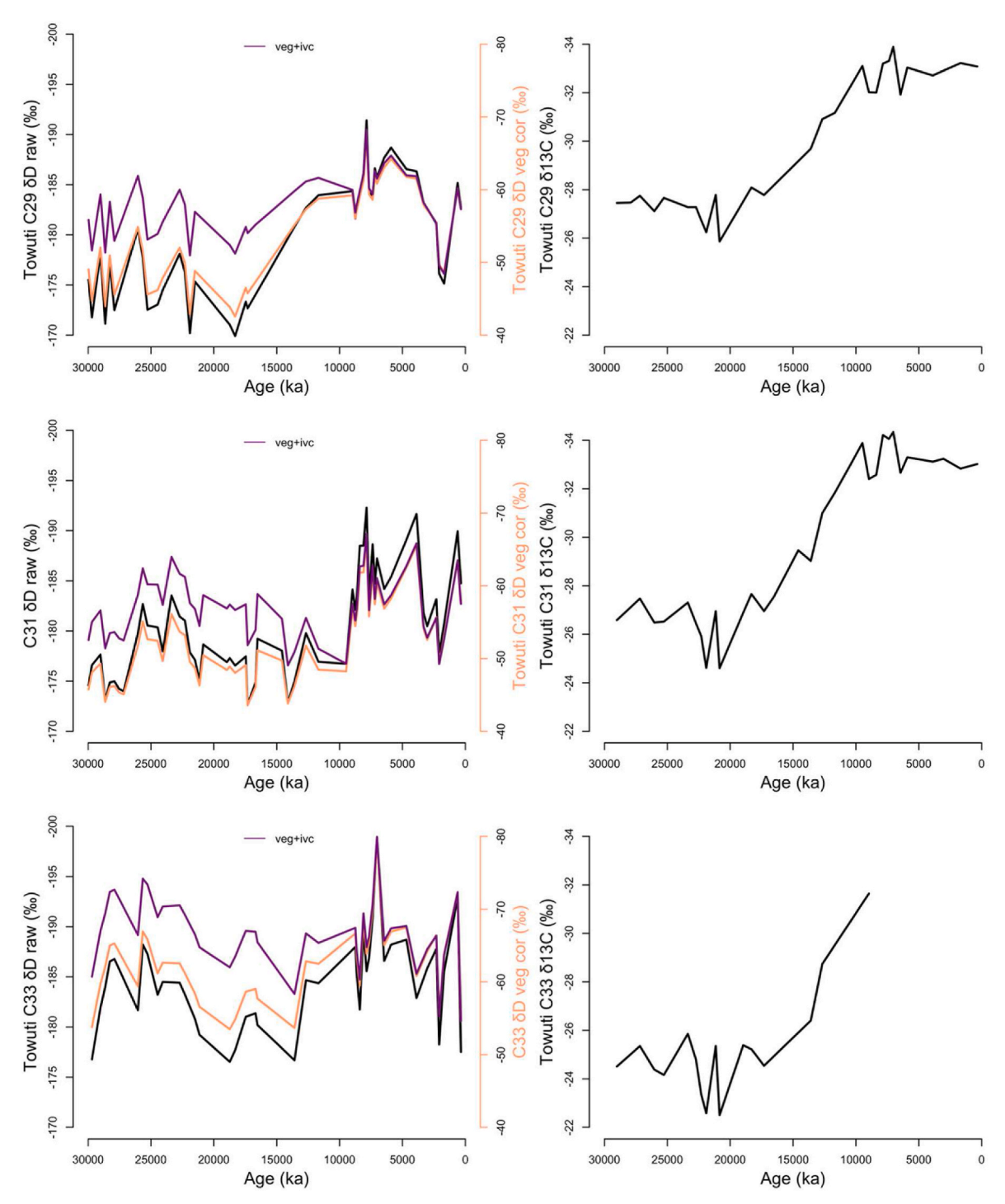


Fig. A.7. Raw  $\delta^2 H_{wax}$  of  $C_{29}$ ,  $C_{31}$ , and  $C_{33}$  alkanes measured from Lake Towuti (black), vegetation corrected using an end-member mixing model described in Konecky et al. (2016) (orange), and vegetation and ice volume corrected (purple).  $\delta^{13} C_{wax}$  of  $C_{29}$ ,  $C_{31}$ , and  $C_{33}$  alkanes measured from Lake Towuti.

### References

Adler, R.F., Sapiano, M.R.P., Huffman, G.J., Wang, J.-J., Gu, G., Bolvin, D., Chiu, L., Schneider, U., Becker, A., Nelkin, E., Xie, P., Ferraro, R., Shin, D.-B., 2018. The global precipitation Climatology Project (GPCP) monthly analysis (new version 2.3) and a review of 2017 global precipitation. Atmosphere 9, 138. https://doi.org/10.3390/atmos9040138.

Ayliffe, L.K., Gagan, M.K., Zhao, J., Drysdale, R.N., Hellstrom, J.C., Hantoro, W.S., Griffiths, M.L., Scott-Gagan, H., Pierre, E.S., Cowley, J.A., Suwargadi, B.W., 2013. Rapid interhemispheric climate links via the Australasian monsoon during the last deglaciation. Nat. Commun. 4, 2908. https://doi.org/10.1038/ncomms3908.

Blaauw, M., Christen, J.A., 2011. Flexible paleoclimate age-depth models using an autoregressive gamma process. Bayesian Analysis 6, 457–474. https://doi.org/ 10.1214/11-BA618.

Brady, E., Stevenson, S., Bailey, D., Liu, Z., Noone, D., Nusbaumer, J., Otto-Bliesner, B.L., Tabor, C., Tomas, R., Wong, T., Zhang, J., Zhu, J., 2019. The Connected isotopic water cycle in the Community Earth system model version 1. J. Adv. Model. Earth Syst. 11, 2547–2566. https://doi.org/10.1029/2019MS001663.

Bray, E.E., Evans, E.D., 1965. Hydrocarbons in non-Reservoir-Rock source Beds1. AAPG (Am. Assoc. Pet. Geol.) Bull. 49, 248–257. https://doi.org/10.1306/A663352E-16C0-11D7-8645000102C1865D.

Bruhl, J., Wilson, K., 2007. Towards a Comprehensive Survey of C3 and C4 photosynthetic pathways in Cyperaceae. Aliso: A Journal of Systematic and Floristic Botany 23, 99–148. https://doi.org/10.5642/aliso.20072301.11.

- Chikaraishi, Y., Naraoka, H., 2007. δ13C and δD relationships among three n-alkyl compound classes (n-alkanoic acid, n-alkane and n-alkanol) of terrestrial higher plants. Org. Geochem. 38, 198–215. https://doi.org/10.1016/j.orggeochem.2006.10.003.
- Contreras, S., Werne, J.P., Araneda, A., Tejos, E., Moscoso, J., 2023. Abundance and distribution of plant derived leaf waxes (long chain n-alkanes & fatty acids) from lake surface sediments along the west coast of southern South America: implications for environmental and climate reconstructions. Sci. Total Environ. 895, 165065 https://doi.org/10.1016/j.scitotenv.2023.165065.
- Costa, K.M., Russell, J.M., Vogel, H., Bijaksana, S., 2015. Hydrological connectivity and mixing of Lake Towuti, Indonesia in response to paleoclimatic changes over the last 60,000years. Palaeogeogr. Palaeoclimatol. Palaeoecol. 417, 467–475. https://doi. org/10.1016/j.palaeo.2014.10.009.
- Diefendorf, A.F., Mueller, K.E., Wing, Scottl., Koch, P.L., Freeman, K.H., 2010. Global patterns in leaf 13C discrimination and implications for studies of past and future climate. Proc. Natl. Acad. Sci. USA 107, 5738–5743. https://doi.org/10.1073/pngs.0910513107
- DiNezio, P.N., Tierney, J.E., 2013. The effect of sea level on glacial Indo-Pacific climate. Nature Geosci 6, 485–491. https://doi.org/10.1038/ngeo1823.
- DiNezio, P.N., Tierney, J.E., Otto-Bliesner, B.L., Timmermann, A., Bhattacharya, T., Rosenbloom, N., Brady, E., 2018. Glacial changes in tropical climate amplified by the Indian Ocean. Sci. Adv. 4, eaat9658. https://doi.org/10.1126/sciadv.aat9658.
- DiNezio, P.N., Timmermann, A., Tierney, J.L., Jin, F.-F., Otto-Bliesner, B., Rosenbloom, N., Mapes, B., Neale, R., Ivanovic, R.F., Montenegro, A., 2016. The climate response of the Indo-Pacific warm pool to glacial sea level. Paleoceanography 31, 866–894. https://doi.org/10.1002/2015PA002890.
- Du, X., Russell, J.M., Liu, Z., Otto-Bliesner, B.L., Gao, Y., Zhu, C., Oppo, D.W., Mohtadi, M., Yan, Y., Galy, V.V., He, C., 2021. Deglacial trends in Indo-Pacific warm pool hydroclimate in an isotope-enabled Earth system model and implications for isotope-based paleoclimate reconstructions. Quat. Sci. Rev. 270, 107188 https://doi. org/10.1016/j.quascirev.2021.107188.
- Dubois, N., Oppo, D.W., Galy, V.V., Mohtadi, M., van der Kaars, S., Tierney, J.E., Rosenthal, Y., Eglinton, T.I., Lückge, A., Linsley, B.K., 2014. Indonesian vegetation response to changes in rainfall seasonality over the past 25,000 years. Nat. Geosci. 7, 513–517. https://doi.org/10.1038/ngeo2182.
- Fan, W., Jian, Z., Chu, Z., Dang, H., Wang, Y., Bassinot, F., Han, X., Bian, Y., 2018.
  Variability of the Indonesian Throughflow in the Makassar strait over the last 30 ka.
  Sci. Rep. 8, 5678. https://doi.org/10.1038/s41598-018-24055-1.
- Feakins, S.J., Bentley, L.P., Salinas, N., Shenkin, A., Blonder, B., Goldsmith, G.R., Ponton, C., Arvin, L.J., Wu, M.S., Peters, T., West, A.J., Martin, R.E., Enquist, B.J., Asner, G.P., Malhi, Y., 2016. Plant leaf wax biomarkers capture gradients in hydrogen isotopes of precipitation from the Andes and Amazon. Geochem. Cosmochim. Acta 182, 155–172. https://doi.org/10.1016/j.gca.2016.03.018.
- Fraser, N., Kuhnt, W., Holbourn, A., Bolliet, T., Andersen, N., Blanz, T., Beaufort, L., 2014. Precipitation variability within the west Pacific warm pool over the past 120 ka: evidence from the Davao Gulf, southern Philippines. Paleoceanography 29, 1094–1110. https://doi.org/10.1002/2013PA002599.
- Garelick, S., Russell, J.M., Dee, S., Verschuren, D., Olago, D.O., 2021. Atmospheric controls on precipitation isotopes and hydroclimate in high-elevation regions in Eastern Africa since the Last Glacial Maximum. Earth Planet Sci. Lett. 567, 116984 https://doi.org/10.1016/j.epsl.2021.116984.
- Gibbons, F.T., Oppo, D.W., Mohtadi, M., Rosenthal, Y., Cheng, J., Liu, Z., Linsley, B.K., 2014. Deglacial 8180 and hydrologic variability in the tropical Pacific and Indian Oceans. Earth Planet Sci. Lett. 387, 240–251. https://doi.org/10.1016/j. epsl.2013.11.032.
- Griffiths, M.L., Drysdale, R.N., Gagan, M.K., Zhao, J. -x, Ayliffe, L.K., Hellstrom, J.C., Hantoro, W.S., Frisia, S., Feng, Y. -x, Cartwright, I., Pierre, E.S., Fischer, M.J., Suwargadi, B.W., 2009. Increasing Australian–Indonesian monsoon rainfall linked to early Holocene sea-level rise. Nat. Geosci. 2, 636–639. https://doi.org/10.1038/ ngeo605.
- Hällberg, P.L., Schenk, F., Yamoah, K.A., Kuang, X., Smittenberg, R.H., 2022. Seasonal aridity in the Indo-Pacific warm pool during the late glacial driven by El Niño-like conditions. Clim. Past 18, 1655–1674. https://doi.org/10.5194/cp-18-1655-2022.
- Hamilton, R., Stevenson, J., Li, B., Bijaksana, S., 2019. A 16,000-year record of climate, vegetation and fire from Wallacean lowland tropical forests. Quat. Sci. Rev. 224, 105929 https://doi.org/10.1016/j.quascirev.2019.105929.
- Hanebuth, T., Stattegger, K., Grootes, P.M., 2000. Rapid flooding of the Sunda shelf: a late-glacial sea-level record. Science 288, 1033–1035. https://doi.org/10.1126/ science.288.5468.1033.
- Hanebuth, T.J.J., Voris, H.K., Yokoyama, Y., Saito, Y., Okuno, J., 2011. Formation and fate of sedimentary depocentres on Southeast Asia's Sunda Shelf over the past sealevel cycle and biogeographic implications. Earth Sci. Rev. 104, 92–110. https://doi. org/10.1016/j.earscirev.2010.09.006.
- He, C., Liu, Z., Otto-Bliesner, B.L., Brady, E.C., Zhu, C., Tomas, R., Clark, P.U., Zhu, J., Jahn, A., Gu, S., Zhang, J., Nusbaumer, J., Noone, D., Cheng, H., Wang, Y., Yan, M., Bao, Y., 2021. Hydroclimate footprint of pan-Asian monsoon water isotope during the last deglaciation. Sci. Adv. 7, eabe2611 https://doi.org/10.1126/sciadv.abe2611
- Hijmans, R.J., Etten, J. van, Sumner, M., Cheng, J., Baston, D., Bevan, A., Bivand, R., Busetto, L., Canty, M., Fasoli, B., Forrest, D., Ghosh, A., Golicher, D., Gray, J., Greenberg, J.A., Hiemstra, P., Hingee, K., Ilich, A., Geosciences, I., for, M.A., Karney, C., Mattiuzzi, M., Mosher, S., Naimi, B., Nowosad, J., Pebesma, E., Lamigueiro, O.P., Racine, E.B., Rowlingson, B., Shortridge, A., Venables, B., Wueest, R., 2022. Raster: Geographic Data Analysis and Modeling.
- Hollstein, M., Mohtadi, M., Rosenthal, Y., Prange, M., Oppo, D.W., Martínez Méndez, G., Tachikawa, K., Moffa Sanchez, P., Steinke, S., Hebbeln, D., 2018. Variations in

- Western Pacific Warm Pool surface and thermocline conditions over the past 110,000 years: forcing mechanisms and implications for the glacial Walker circulation. Quat. Sci. Rev. 201, 429–445. https://doi.org/10.1016/j. quascirev.2018.10.030.
- Hope, G., 2001. Environmental change in the late Pleistocene and later Holocene at Wanda site, Soroako, South Sulawesi, Indonesia. Palaeogeography, Palaeoclimatology, Palaeoecology, Quaternary Environmental Change in the Indonesian Region 171, 129–145. https://doi.org/10.1016/S0031-0182(01)00243-7
- Hou, J., D'Andrea, W.J., Huang, Y., 2008. Can sedimentary leaf waxes record D/H ratios of continental precipitation? Field, model, and experimental assessments. Geochem. Cosmochim. Acta 72, 3503–3517. https://doi.org/10.1016/j.gca.2008.04.030.
- Hutchings, J., Konecky, B.L., 2022. Improved Forward Models of Leaf Wax Hydrogen Isotope Ratios from a Synthesis of 3,500+ Measurements in Modern Plants 2022, pp. PP32D-972.
- Hutchings, J., Konecky, B.L., 2020. Phylogenetic, Adaptational, and Environmental Controls on Hydrogen Isotope Apparent Fractionation in Leaf Waxes from a Synthesis of 3,000+ Plant Specimens 2020. PP006-01.
- Iturbide, M., Gutiérrez, J.M., Alves, L.M., Bedia, J., Cerezo-Mota, R., Cimadevilla, E., Cofiño, A.S., Di Luca, A., Faria, S.H., Gorodetskaya, I.V., Hauser, M., Herrera, S., Hennessy, K., Hewitt, H.T., Jones, R.G., Krakovska, S., Manzanas, R., Martínez-Castro, D., Narisma, G.T., Nurhati, I.S., Pinto, I., Seneviratne, S.I., van den Hurk, B., Vera, C.S., 2020. An update of IPCC climate reference regions for subcontinental analysis of climate model data: definition and aggregated datasets. Earth Syst. Sci. Data 12, 2959–2970. https://doi.org/10.5194/essd-12-2959-2020.
- Jiang, Y., Zhou, L., Tucker, C.J., Raghavendra, A., Hua, W., Liu, Y.Y., Joiner, J., 2019.
  Widespread increase of boreal summer dry season length over the Congo rainforest.
  Nat. Clim. Chang. 9, 617–622. https://doi.org/10.1038/s41558-019-0512-y.
- Kalnay, E., Kanamitsu, M., Kistler, R., Collins, W., Deaven, D., Gandin, L., Iredell, M., Saha, S., White, G., Woollen, J., Zhu, Y., Chelliah, M., Ebisuzaki, W., Higgins, W., Janowiak, J., Mo, K.C., Ropelewski, C., Wang, J., Leetmaa, A., Reynolds, R., Jenne, R., Joseph, D., 1996. The NCEP/NCAR 40-year reanalysis Project. Bull. Am. Meteorol. Soc. 77, 437–472. https://doi.org/10.1175/1520-0477(1996)077<0437: TNYRP>2.0.CO;2.
- Killick, R., Beaulieu, C., Taylor, S., Hullait, H., 2021. EnvCpt: Detection of Structural Changes in Climate and Environment Time Series.
- Kimbrough, A.K., Gagan, M.K., Dunbar, G.B., Hantoro, W.S., Shen, C.-C., Hu, H.-M., Cheng, H., Edwards, R.L., Rifai, H., Suwargadi, B.W., 2023. Multi-proxy validation of glacial-interglacial rainfall variations in southwest Sulawesi. Commun Earth Environ 4, 1–13. https://doi.org/10.1038/s43247-023-00873-8.
- Konecky, B., Russell, J., Bijaksana, S., 2016. Glacial aridity in central Indonesia coeval with intensified monsoon circulation. Earth Planet Sci. Lett. 437, 15–24. https://doi. org/10.1016/j.epsl.2015.12.037.
- Konecky, B.L., Noone, D.C., Cobb, K.M., 2019. The influence of competing hydroclimate processes on stable isotope ratios in tropical rainfall. Geophys. Res. Lett. 46, 1622–1633. https://doi.org/10.1029/2018GL080188.
- Krause, C.E., Gagan, M.K., Dunbar, G.B., Hantoro, W.S., Hellstrom, J.C., Cheng, H., Edwards, R.L., Suwargadi, B.W., Abram, N.J., Rifai, H., 2019. Spatio-temporal evolution of Australasian monsoon hydroclimate over the last 40,000 years. Earth Planet Sci. Lett. 513, 103–112. https://doi.org/10.1016/j.epsl.2019.01.045.
- Kuechler, R.R., Schefuß, E., Beckmann, B., Dupont, L., Wefer, G., 2013. NW African hydrology and vegetation during the Last Glacial cycle reflected in plant-waxspecific hydrogen and carbon isotopes. Quat. Sci. Rev. 82, 56–67. https://doi.org/ 10.1016/j.quascirev.2013.10.013.
- Lambeck, K., Rouby, H., Purcell, A., Sun, Y., Sambridge, M., 2014. Sea Level and Global Ice Volumes from the Last Glacial Maximum to the Holocene, vol. 111. Proceedings of the National Academy of Sciences, pp. 15296–15303. https://doi.org/10.1073/ pnas.1411762111
- Levi, C., Labeyrie, L., Bassinot, F., Guichard, F., Cortijo, E., Waelbroeck, C., Caillon, N., Duprat, J., de Garidel-Thoron, T., Elderfield, H., 2007. Low-latitude hydrological cycle and rapid climate changes during the last deglaciation. G-cubed 8. https://doi. org/10.1029/2006GC001514.
- Lewis, S.E., Sloss, C.R., Murray-Wallace, C.V., Woodroffe, C.D., Smithers, S.G., 2013. Post-glacial sea-level changes around the Australian margin: a review. Quaternary Science Reviews, Linking Southern Hemisphere records and past circulation patterns: the AUS-INTIMATE project 74, 115–138. https://doi.org/10.1016/j. quascirev.2012.09.006.
- Lisiecki, L.E., Raymo, M.E., 2005. A Pliocene-Pleistocene stack of 57 globally distributed benthic  $\delta^{18}$  O records: PLIOCENE-PLEISTOCENE BENTHIC STACK. Paleoceanography 20. https://doi.org/10.1029/2004PA001071 n/a-n/a.
- Lupien, R.L., Russell, J.M., Subramanian, A., Kinyanjui, R., Beverly, E.J., Uno, K.T., de Menocal, P., Dommain, R., Potts, R., 2021. Eastern African environmental variation and its role in the evolution and cultural change of Homo over the last 1 million years. J. Hum. Evol. 157, 103028 https://doi.org/10.1016/j.jhevol.2021.103028.
- Marcott, S.A., Bauska, T.K., Buizert, C., Steig, E.J., Rosen, J.L., Cuffey, K.M., Fudge, T.J., Severinghaus, J.P., Ahn, J., Kalk, M.L., McConnell, J.R., Sowers, T., Taylor, K.C., White, J.W.C., Brook, E.J., 2014. Centennial-scale changes in the global carbon cycle during the last deglaciation. Nature 514, 616–619. https://doi.org/10.1038/ nature13799.
- Mohtadi, M., Oppo, D.W., Steinke, S., Stuut, J.-B.W., De Pol-Holz, R., Hebbeln, D., Lückge, A., 2011. Glacial to Holocene swings of the Australian–Indonesian monsoon. Nature Geosci 4, 540–544. https://doi.org/10.1038/ngeo1209.
- Mohtadi, M., Prange, M., Oppo, D.W., De Pol-Holz, R., Merkel, U., Zhang, X., Steinke, S., Lückge, A., 2014. North Atlantic forcing of tropical Indian Ocean climate. Nature 509, 76–80. https://doi.org/10.1038/nature13196.

- Mohtadi, M., Steinke, S., Lückge, A., Groeneveld, J., Hathorne, E.C., 2010. Glacial to Holocene surface hydrography of the tropical eastern Indian Ocean. Earth Planet Sci. Lett. 292, 89–97. https://doi.org/10.1016/j.epsl.2010.01.024.
- Niedermeyer, E.M., Sessions, A.L., Feakins, S.J., Mohtadi, M., 2014. Hydroclimate of the western Indo-Pacific warm pool during the past 24,000 years. Proc. Natl. Acad. Sci. USA 111, 9402–9406. https://doi.org/10.1073/pnas.1323585111.
- O'Mara, N.A., Skonieczny, C., McGee, D., Winckler, G., Bory, A.J.-M., Bradtmiller, L.I., Malaizé, B., Polissar, P.J., 2022. Pleistocene drivers of Northwest African hydroclimate and vegetation. Nat. Commun. 13, 3552. https://doi.org/10.1038/s41467-002-31120-x
- Pagani, M., Freeman, K.H., Arthur, M.A., 1999. Late Miocene atmospheric CO2 concentrations and the expansion of C4 grasses. Science 285, 876–879. https://doi. org/10.1126/science.285.5429.876.
- Parish, M.C., Du, X., Bijaksana, S., Russell, J.M., 2023. A brGDGT-based reconstruction of terrestrial temperature from the Maritime continent spanning the last glacial maximum. Paleoceanogr. Paleoclimatol. 38, e2022PA004501 https://doi.org/ 10.1029/2022PA004501.
- Partin, J.W., Cobb, K.M., Adkins, J.F., Clark, B., Fernandez, D.P., 2007. Millennial-scale trends in west Pacific warm pool hydrology since the Last Glacial Maximum. Nature 449, 452–455. https://doi.org/10.1038/nature06164.
- Pico, T., McGee, D., Russell, J., Mitrovica, J.X., 2020. Recent constraints on MIS 3 sea level support role of continental shelf exposure as a control on Indo-Pacific hydroclimate. Paleoceanogr. Paleoclimatol. 35 https://doi.org/10.1029/ 2020PA003998
- Reeves, J.M., Bostock, H.C., Ayliffe, L.K., Barrows, T.T., De Deckker, P., Devriendt, L.S., Dunbar, G.B., Drysdale, R.N., Fitzsimmons, K.E., Gagan, M.K., Griffiths, M.L., Haberle, S.G., Jansen, J.D., Krause, C., Lewis, S., McGregor, H.V., Mooney, S.D., Moss, P., Nanson, G.C., Purcell, A., van der Kaars, S., 2013. Palaeoenvironmental change in tropical Australasia over the last 30,000 years a synthesis by the OZ-INTIMATE group. Quaternary Science Reviews, Linking Southern Hemisphere records and past circulation patterns: the AUS-INTIMATE project 74, 97–114. https://doi.org/10.1016/j.guascirev.2012.11.027.
- Rosenthal, Y., Oppo, D.W., Linsley, B.K., 2003. The amplitude and phasing of climate change during the last deglaciation in the Sulu Sea, western equatorial Pacific: the amplitude and phasing of climate change. Geophys. Res. Lett. 30 https://doi.org/ 10.1029/200261016612.
- Ruan, Y., Mohtadi, M., van der Kaars, S., Dupont, L.M., Hebbeln, D., Schefuß, E., 2019. Differential hydro-climatic evolution of East Javanese ecosystems over the past 22,000 years. Quat. Sci. Rev. 218, 49–60. https://doi.org/10.1016/j. quascirev.2019.06.015.
- Russell, J.M., Vogel, H., Bijaksana, S., Melles, M., Deino, A., Haffidz, A., Haffner, D., Hasberg, A.K.M., Morlock, M., von Rintelen, T., Sheppard, R., Stelbrink, B., Stevenson, J., 2020. The late quaternary tectonic, biogeochemical, and environmental evolution of ferruginous Lake Towuti, Indonesia. Palaeogeogr. Palaeoclimatol. Palaeoecol. 556, 109905 https://doi.org/10.1016/j.palaeo.2020.109905.
- Russell, J.M., Vogel, H., Konecky, B.L., Bijaksana, S., Huang, Y., Melles, M., Wattrus, N., Costa, K., King, J.W., 2014. Glacial forcing of central Indonesian hydroclimate since 60. 000 y B.P. PNAS 111, 5100–5105. https://doi.org/10.1073/pnas.1402373111.
- Sachse, D., Billault, I., Bowen, G.J., Chikaraishi, Y., Dawson, T.E., Feakins, S.J., Freeman, K.H., Magill, C.R., McInerney, F.A., Van Der Meer, M.T.J., Polissar, P., Robins, R.J., Sachs, J.P., Schmidt, H.L., Sessions, A.L., White, J.W.C., West, J.B., Kahmen, A., 2012. Molecular paleohydrology: Interpreting the hydrogen-isotopic composition of lipid biomarkers from photosynthesizing organisms. Annu. Rev. Earth Planet Sci. 40, 221–249. https://doi.org/10.1146/annurev-earth-042711-105535.
- Sarnthein, M., Grootes, P.M., Holbourn, A., Kuhnt, W., Kühn, H., 2011. Tropical warming in the Timor Sea led deglacial Antarctic warming and atmospheric CO2 rise by more than 500yr. Earth Planet Sci. Lett. 302, 337–348. https://doi.org/10.1016/j. epsl.2010.12.021.
- Schrag, D.P., Hampt, G., Murray, D.W., 1996. Pore Fluid constraints on the temperature and oxygen isotopic composition of the glacial ocean. Science 272, 1930–1932. https://doi.org/10.1126/science.272.5270.1930.
- Schröder, J.F., Kuhnt, W., Holbourn, A., Beil, S., Zhang, P., Hendrizan, M., Xu, J., 2018. Deglacial warming and hydroclimate variability in the central Indonesian

- Archipelago. Paleoceanogr. Paleoclimatol. 33, 974–993. https://doi.org/10.1029/2018PA003323.
- Stott, L., Poulsen, C., Lund, S., Thunell, R., 2002. Super ENSO and global climate oscillations at millennial time scales. Science 297, 222–226. https://doi.org/10.1126/science.1071627.
- Stott, L., Timmermann, A., Thunell, R., 2007. Southern Hemisphere and Deep-sea warming led deglacial atmospheric CO2 rise and tropical warming. Science 318, 435–438. https://doi.org/10.1126/science.1143791.
- Tierney, J.E., Oppo, D.W., LeGrande, A.N., Huang, Y., Rosenthal, Y., Linsley, B.K., 2012. The influence of Indian Ocean atmospheric circulation on Warm Pool hydroclimate during the Holocene epoch. J. Geophys. Res. Atmos. 117 https://doi.org/10.1029/ 2012.JD018060.
- van Bree, L.G.J., Peterse, F., van der Meer, M.T.J., Middelburg, J.J., Negash, A.M.D., De Crop, W., Cocquyt, C., Wieringa, J.J., Verschuren, D., Sinninghe Damsté, J.S., 2018. Seasonal variability in the abundance and stable carbon-isotopic composition of lipid biomarkers in suspended particulate matter from a stratified equatorial lake (Lake Chala, Kenya/Tanzania): implications for the sedimentary record. Quat. Sci. Rev. 192, 208–224. https://doi.org/10.1016/j.quascirev.2018.05.023.
- van der Kaars, S., Bassinot, F., De Deckker, P., Guichard, F., 2010. Changes in monsoon and ocean circulation and the vegetation cover of southwest Sumatra through the last 83,000years: the record from marine core BAR94-42. Palaeogeogr. Palaeoclimatol. Palaeoecol. 296, 52–78. https://doi.org/10.1016/j. palaeo.2010.06.015.
- van der Kaars, S., Penny, D., Tibby, J., Fluin, J., Dam, R.A.C., Suparan, P., 2001. Late Quaternary palaeoecology, palynology and palaeolimnology of a tropical lowland swamp: Rawa Danau, West-Java, Indonesia. Palaeogeography, Palaeoclimatology, Palaeoecology, Quaternary Environmental Change in the Indonesian Region 171, 185–212. https://doi.org/10.1016/S0031-0182(01)00245-0.
- van der Kaars, S., Wang, X., Kershaw, P., Guichard, F., Setiabudi, D.A., 2000. A Late Quaternary palaeoecological record from the Banda Sea, Indonesia: patterns of vegetation, climate and biomass burning in Indonesia and northern Australia. Palaeogeogr. Palaeoclimatol. Palaeoecol. 155, 135–153. https://doi.org/10.1016/S0031-0182(99)00098-X.
- Visser, K., Thunell, R., Stott, L., 2003. Magnitude and timing of temperature change in the Indo-Pacific warm pool during deglaciation. Nature 421, 152–155. https://doi. org/10.1038/nature01297.
- Vogel, H., Russell, J.M., Cahyarini, S.Y., Bijaksana, S., Wattrus, N., Rethemeyer, J., Melles, M., 2015. Depositional modes and lake-level variability at Lake Towuti, Indonesia, during the past ~29 kyr BP. J. Paleolimnol. 54, 359–377. https://doi.org/ 10.1007/s10933-015-9857-z.
- Wicaksono, S.A., Russell, J.M., Bijaksana, S., 2015. Compound-specific carbon isotope records of vegetation and hydrologic change in central Sulawesi, Indonesia, since 53,000 yr BP. Palaeogeogr. Palaeoclimatol. Palaeoecol. 430, 47–56. https://doi.org/ 10.1016/j.palaeo.2015.04.016.
- Wicaksono, S.A., Russell, J.M., Holbourn, A., Kuhnt, W., 2017. Hydrological and vegetation shifts in the Wallacean region of central Indonesia since the last glacial maximum. Quat. Sci. Rev. 157, 152–163. https://doi.org/10.1016/j. guascirev.2016.12.006
- Windler, G., Tierney, J.E., DiNezio, P.N., Gibson, K., Thunell, R., 2019. Shelf exposure influence on Indo-Pacific Warm Pool climate for the last 450,000 years. Earth Planet Sci. Lett. 516, 66–76. https://doi.org/10.1016/j.epsl.2019.03.038.
- Wurster, C.M., Rifai, H., Zhou, B., Haig, J., Bird, M.I., 2019. Savanna in equatorial Borneo during the late Pleistocene. Sci. Rep. 9, 6392. https://doi.org/10.1038/s41598.019.42670.4
- Wurtzel, J.B., Abram, N.J., Lewis, S.C., Bajo, P., Hellstrom, J.C., Troitzsch, U., Heslop, D., 2018. Tropical Indo-Pacific hydroclimate response to North Atlantic forcing during the last deglaciation as recorded by a speleothem from Sumatra, Indonesia. Earth Planet Sci. Lett. 492, 264–278. https://doi.org/10.1016/j.epsl.2018.04.001.
- Xu, J., Holbourn, A., Kuhnt, W., Jian, Z., Kawamura, H., 2008. Changes in the thermocline structure of the Indonesian outflow during Terminations I and II. Earth Planet Sci. Lett. 273, 152–162. https://doi.org/10.1016/j.epsl.2008.06.029.
- Yuan, S., Chiang, H.-W., Liu, G., Bijaksana, S., He, S., Jiang, X., Imran, A.M., Wicaksono, S.A., Wang, X., 2023. The strength, position, and width changes of the intertropical convergence zone since the Last Glacial Maximum. Proc. Natl. Acad. Sci. USA 120, e2217064120. https://doi.org/10.1073/pnas.2217064120.